

2014 Spring

**“Advanced Physical Metallurgy”
- Bulk Metallic Glasses -**

05.15.2014

Eun Soo Park

Office: 33-313

Telephone: 880-7221

Email: espark@snu.ac.kr

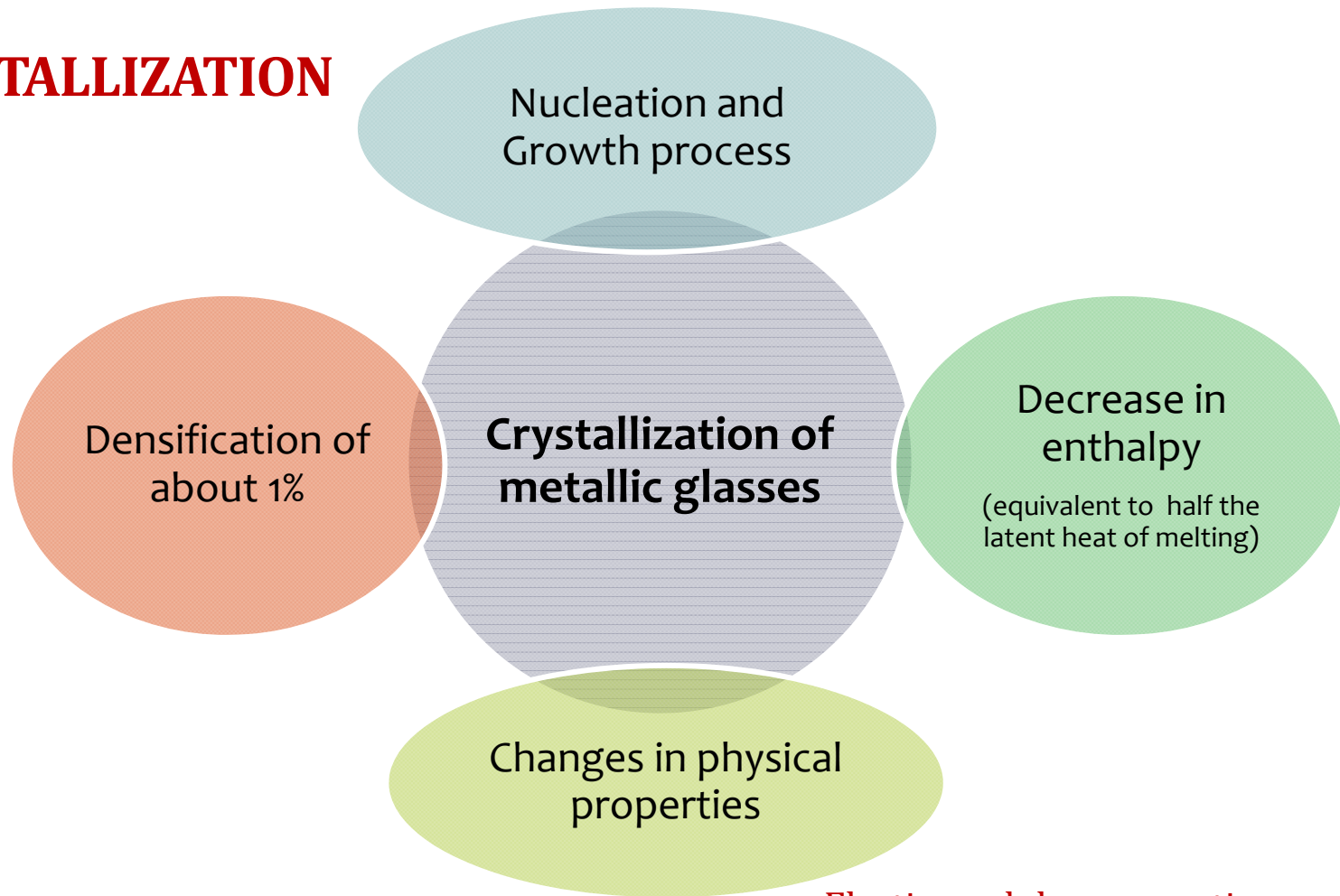
Office hours: by appointment

5 Crystallization Behavior

Temp. or Pressure
↓
Amorphous phase → crystal phase
(high E (metastable) state)

Tailor the microstructure to obtain a glass+nanocrystal or an ultrafine-grained composite, or a completely crystalline materials of different grain sizes by controlling the time and temperature of crystallization.

CRYSTALLIZATION



Elastic modulus, magnetic coercivity

5.2.3 Structural Details

- **Amorphous vs Nanocrystalline**

1) *Microstructural observation*

XRD, (HR)TEM, EXAFS ...

2) *Thermal analysis*

DSC (Differential Scanning Calorimetry)

: Measure heat absorbed or liberated during heating or cooling

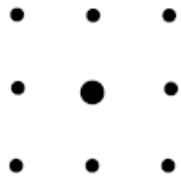
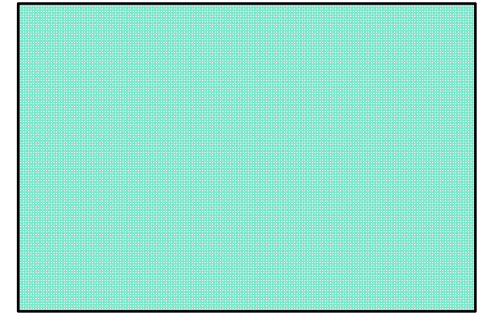
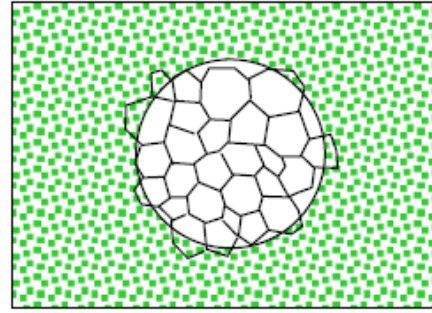
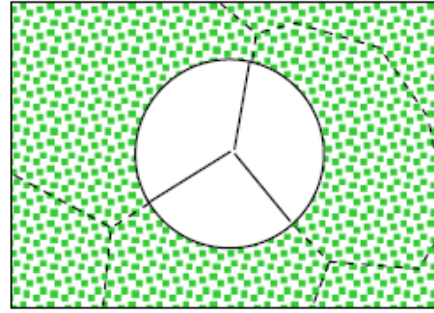
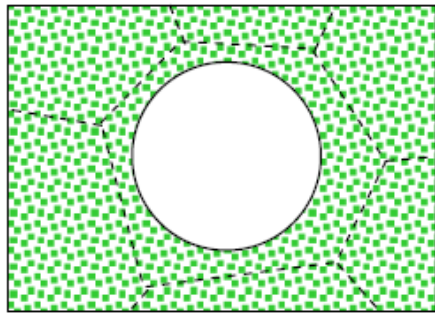
cf) a) glass → nucleation & growth

(perfect random)

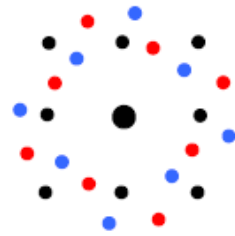
b) local clustering: quenched-in nuclei → only growth

c) Nanocrystalline → growth

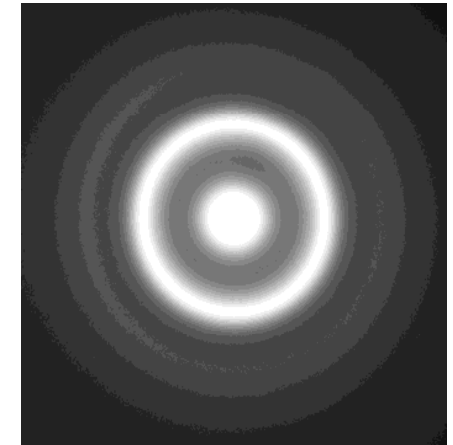
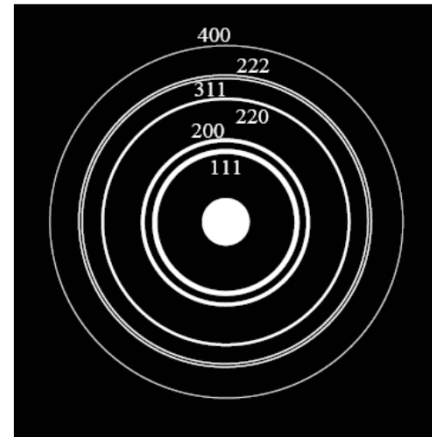
Electron Diffraction Pattern--Spot to Ring



(a)

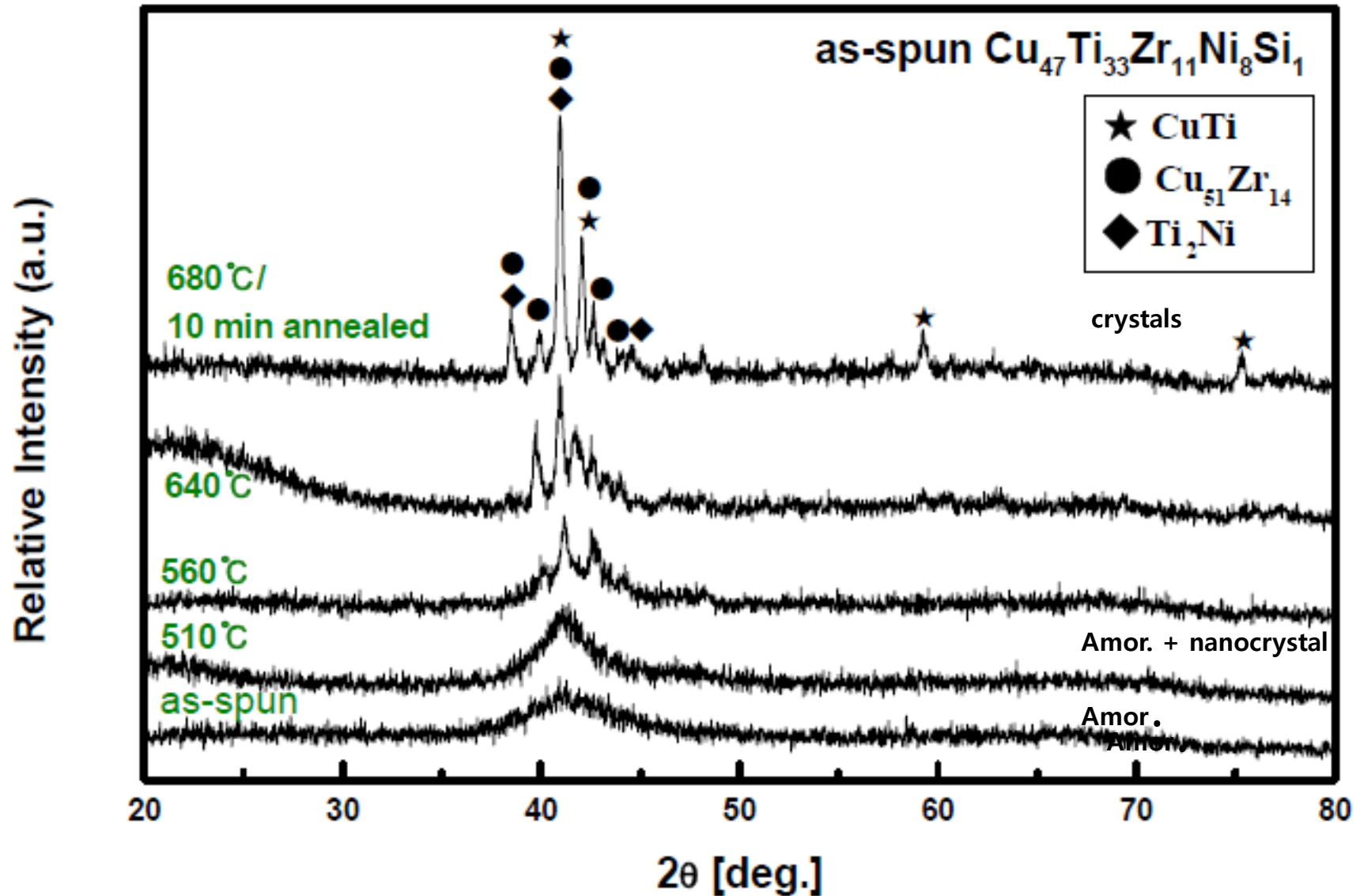


(b)



* X-ray diffraction or Neutron results

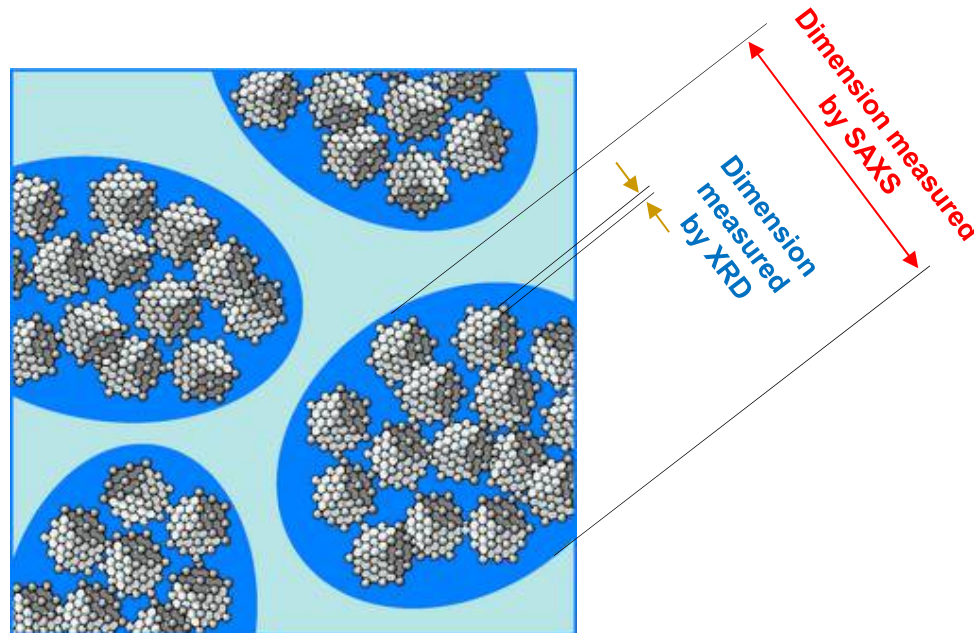
Crystallization after annealing



Angle range of Small angle scattering

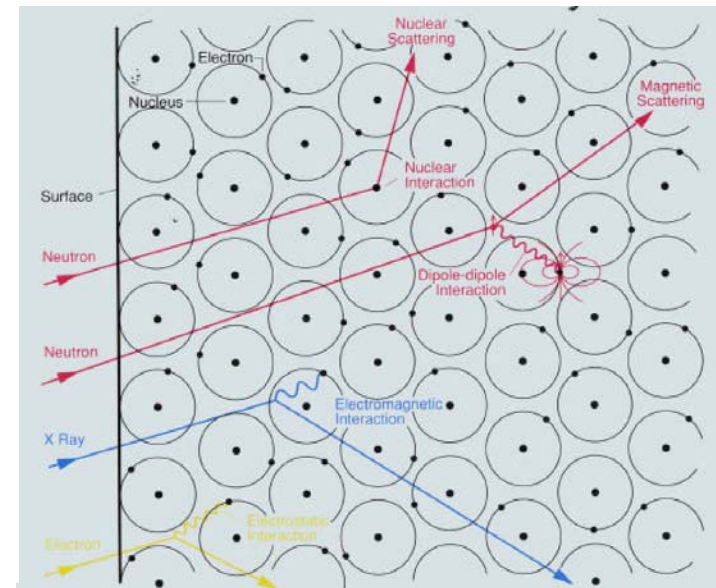
- Length scale of small angle scattering : 1 – 1000 nm
- Information on relatively large r is contained in $I(q)$ at relatively small $q (=4\pi\sin\theta/\lambda)$
- Bragg's law : $\sin\theta = \lambda/2d$

$d = \text{few } \text{\AA}$	$\lambda = 1 \text{ \AA}$	$2\theta = 20$
$d = 100 \text{ \AA}$	$\lambda = 1 \text{ \AA}$	$2\theta = 0.6$
- Sample contains a scattering length density inhomogeneity of dimension larger than 1 nm, scattering becomes observable in small angle region ($0 \sim 4^\circ$)

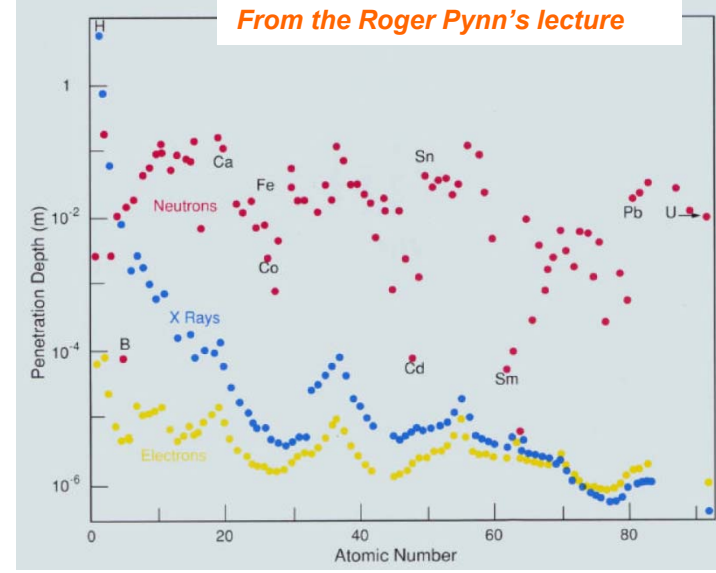


Coherent and Incoherent Scattering

items	X-ray	neutron
source	collision of electrons with target metals(Cu, Mo, W...) acceleration of charged particles	nuclear reactor spallation neutron source (accelerator)
scattered by	electrons	atomic nuclei, unpaired spins
interaction	EM(electromagnetic)	Nuclear(strong int.) EM
scattering amplitude	linearly depend on Z	nearly indep. on Z
sample amount	$\mu\text{g} \sim \text{mg}$	$\sim\text{g}$
meas. time	$10^1\sim 2$ min (step scan: $\sim\text{hr}$)	$10^0\sim 2$ hr
hard to see	relatively light elements (H, Li, B, C, O ...)	highly abs. nuclei (Gd, Sm, Eu, Cd, B...)

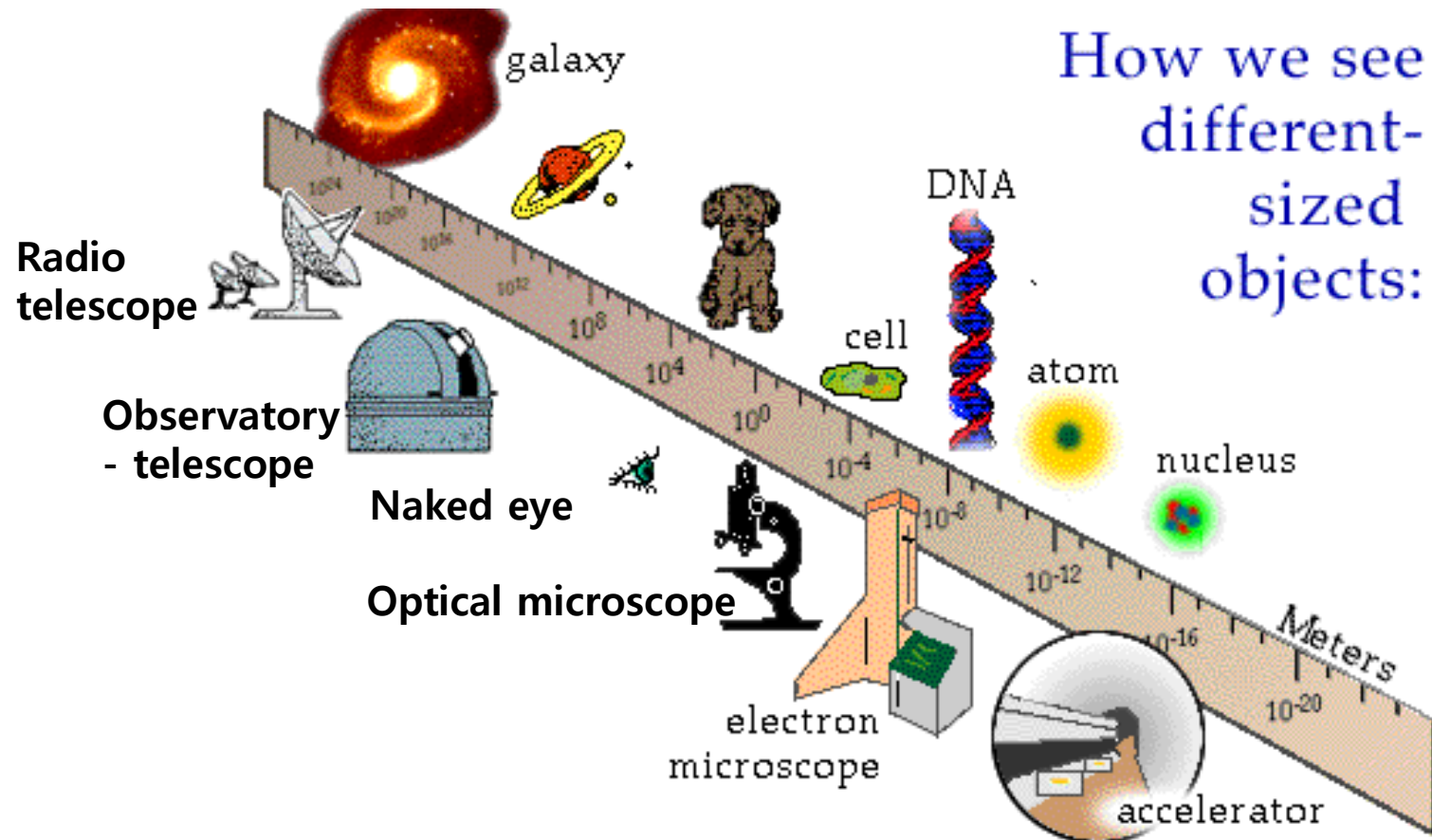


From the Roger Pynn's lecture



High energy particles can be used to reveal the structure of matter!

- To explore matter at its smallest size, we need very high momentum particles !
- “atom-smashers” or “accelerators”

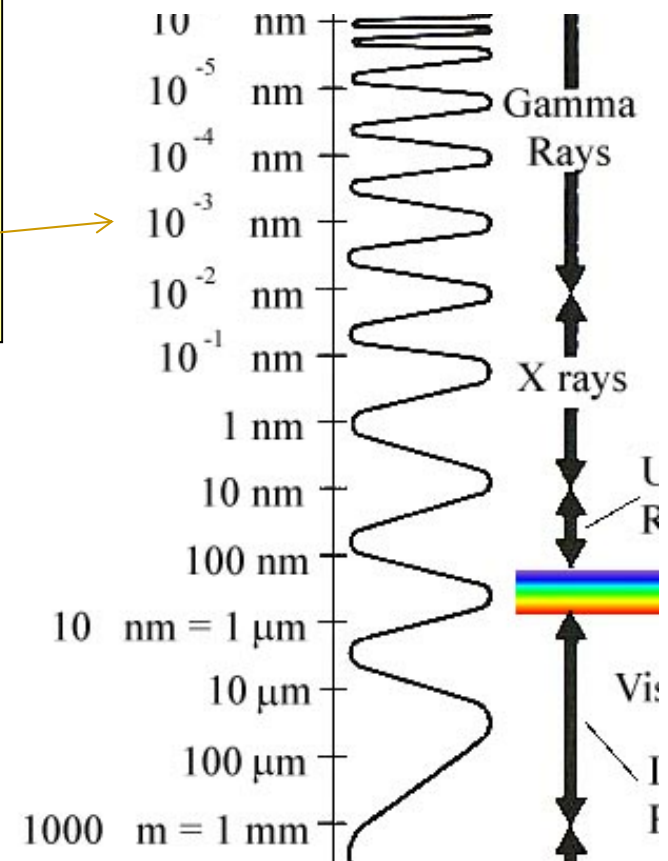


Lowest wavelength by electron

Compute the wavelength of an electron
($m = 9.1 \times 10^{-31}$ [kg]) moving at 3×10^8 [m/s].

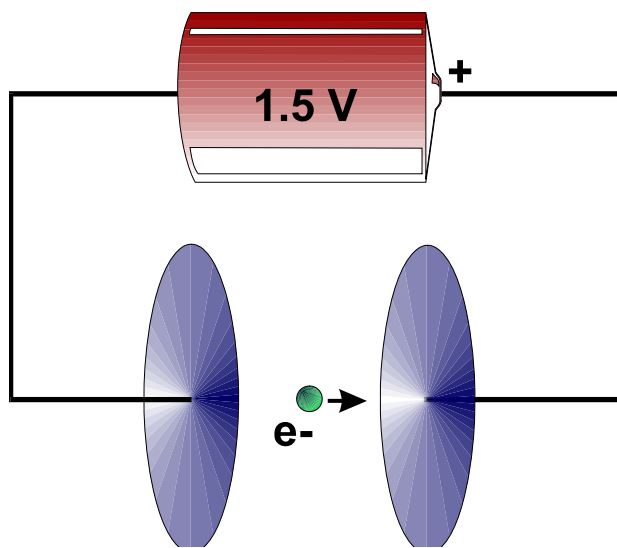
$$\begin{aligned}\lambda &= h/mv \\ &= 6.6 \times 10^{-34} \text{ [J s]} / (9.1 \times 10^{-31} \text{ [kg]})(3 \times 10^8 \text{ [m/s]}) \\ &= 2.43 \times 10^{-12} \text{ [m]} = 2.43 \times 10^{-3} \text{ [nm]} \\ &= \mathbf{0.00243 \text{ [nm]}}\end{aligned}$$

**These electrons have a wavelength
in the region of Gamma-Rays**

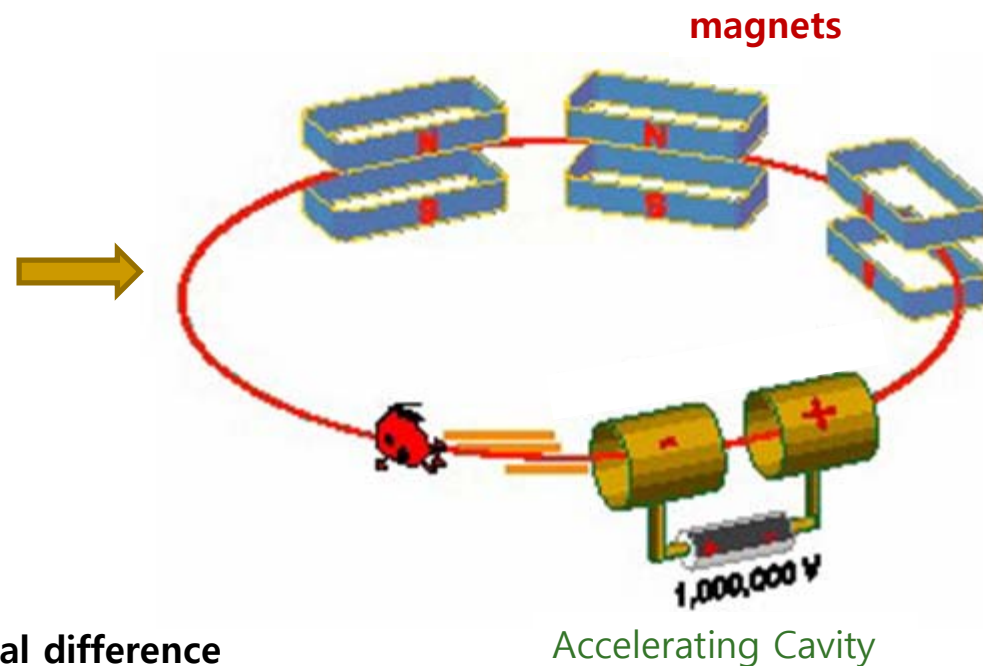


Electric field for acceleration

- Accelerator works for a charged particle such as **electron, proton, etc.**
- **Electric field** : acceleration of charged particle
- **Magnetic field: change of direction**



The single electron passes through a potential difference of 1.5 volts, thus gaining 1.5 electron-volts of energy



Electron: easy to acceleration

		~ 700 km/s
		~2000 km/s
20 000 V		~90 000 km/s
800 000 000 V		299 792.4 <u>0</u> km/s
1 700 000 000 V		299 792.4 <u>4</u> km/s

Close to the light velocity = 299 792 458 m/s

Particle accelerator

- To know atomic structure of matter → need to obtain **simplest kinds of interactions at the highest possible energies**

(development of Rutherford scattering experiment)

- **Photon** with internal structure (quark & gluon) → discovery of new particle

- **Electron** : lowest weight & no internal structure → easy to prediction of generating particles during collision (precision test)/

easy to lose their energy during circular acceleration

- **Linear particle accelerators/ Circular or cyclic accelerators**

(Easy to acceleration with low cost)

- **Synchrotron** → use of synchrotron radiation sources

(light source with various wavelengths, especially low wavelength and high energy)



Pohang accelerators

Structure of Synchrotron

Incident beam generator

Linear accelerator

Rotating electron

Storage ring

magnets

Beamline

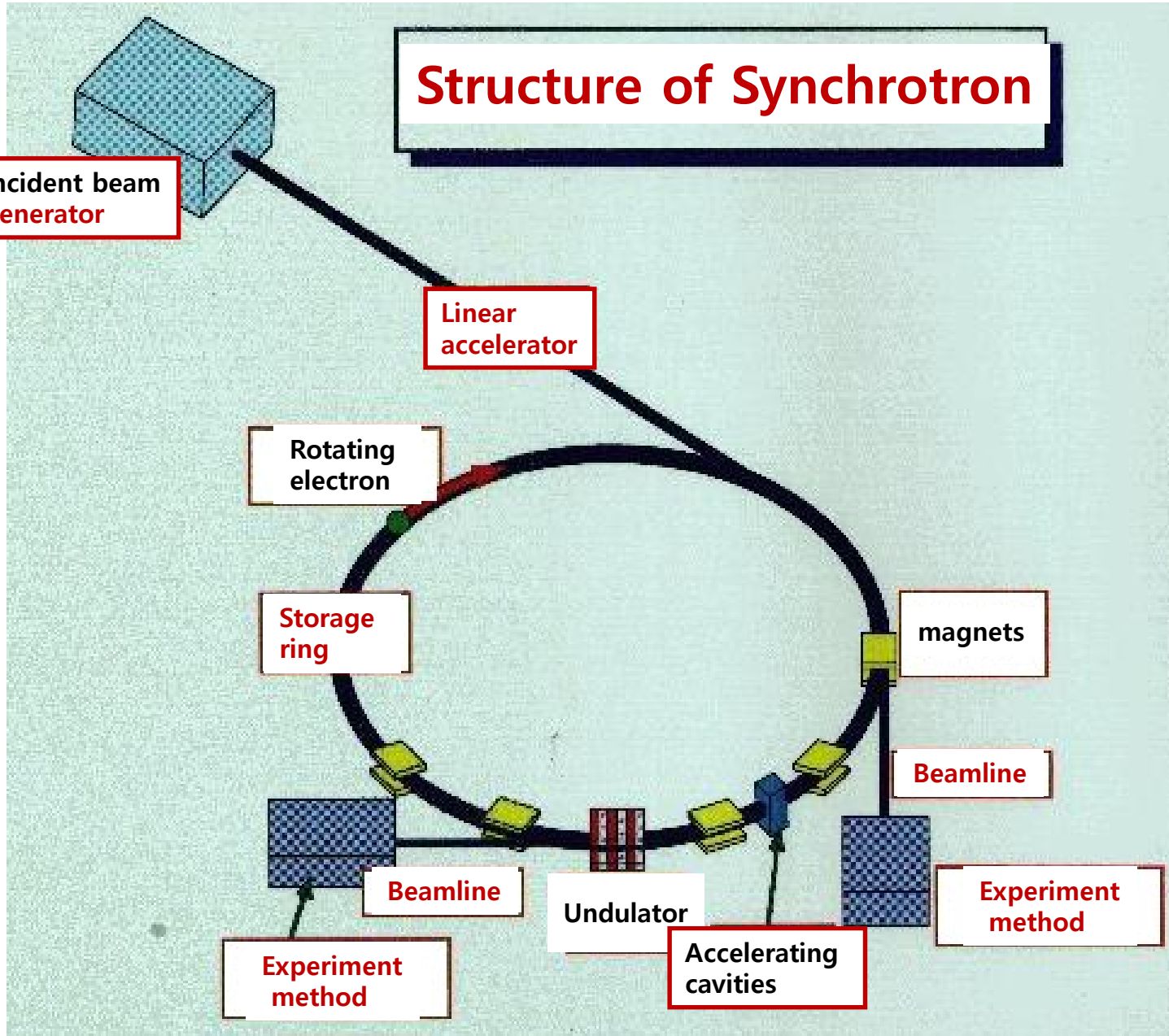
Beamline

Undulator

Accelerating cavities

Experiment method

Experiment method

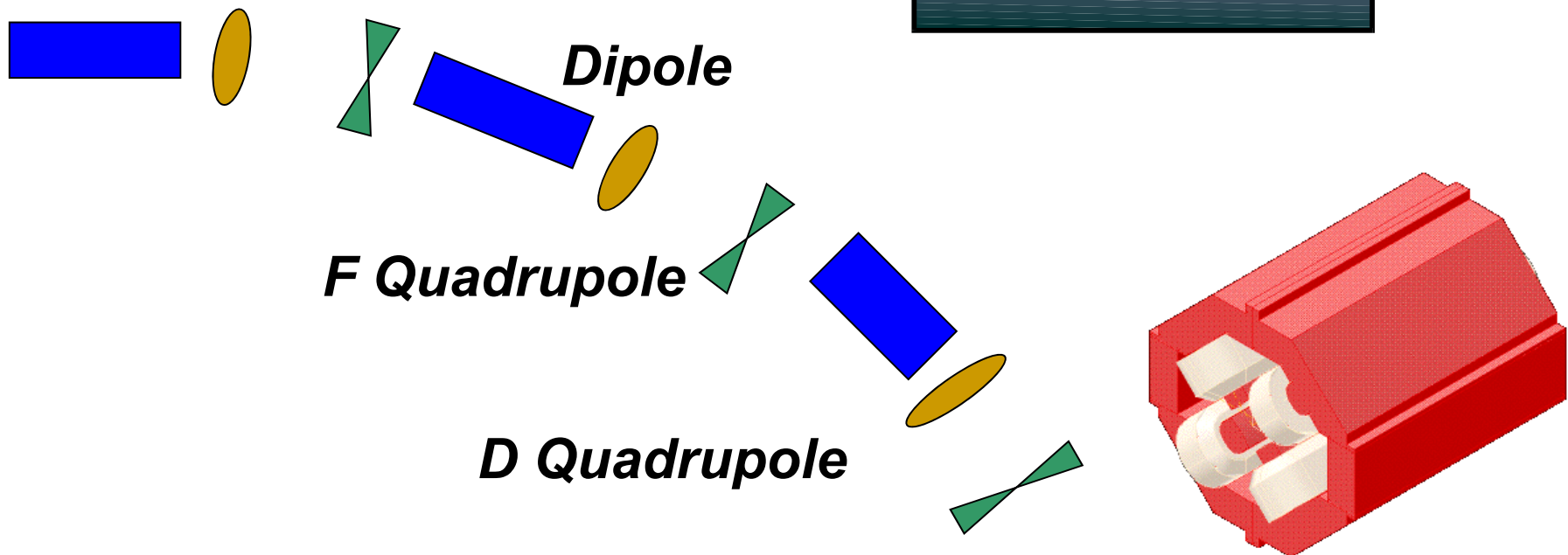
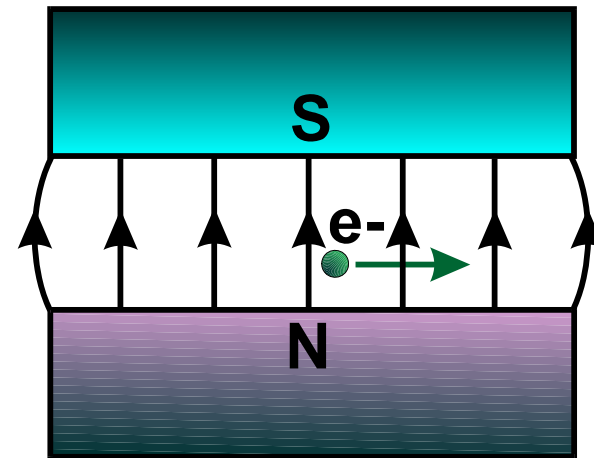


How we manipulate the beam

- The charged particle beam is then manipulated by the use of powerful magnets
- In analogy with light optics, we call this process magnetic beam optics
- The beam is **bent** using dipole magnets and **focusing** using quadrupole magnets
- The magnets are very strong, often several Tesla, and use normal conducting, superconducting or permanent magnet technology

Magnetic lattices

- Magnets are combined to form a magnet lattice
- The lattice steers and focuses the beam

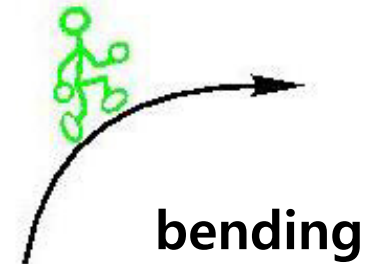
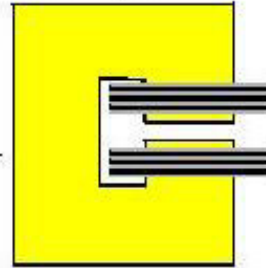


Magnets in storage ring

Base level

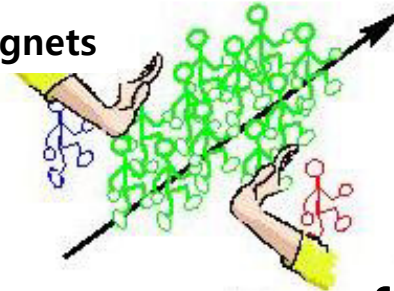


Dipole magnets



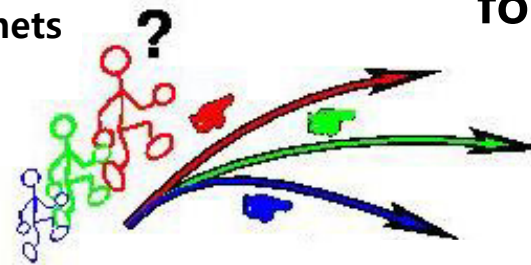
bending

quadrupole magnets



focusing

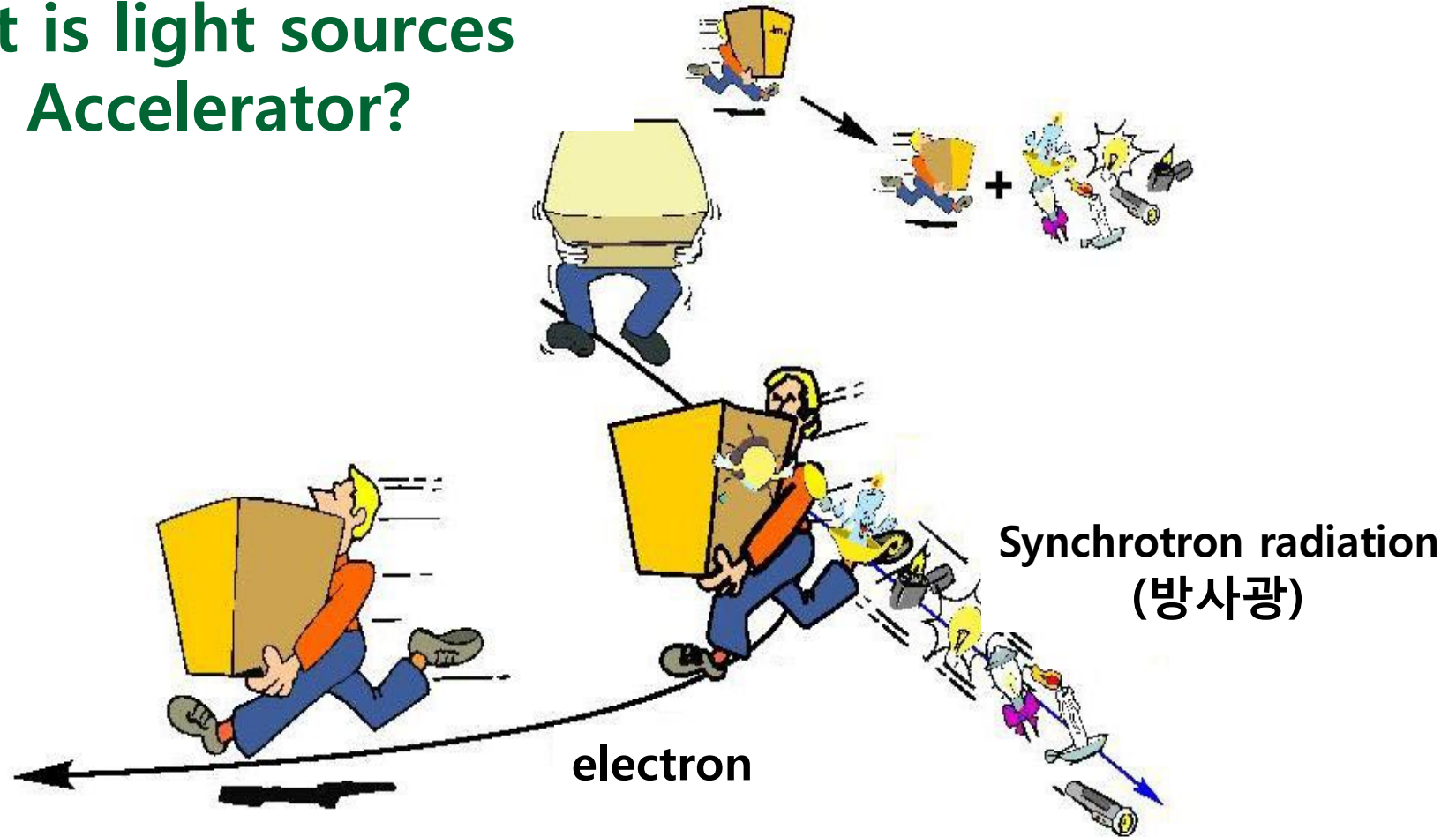
Sextupole magnets



correction
(chromatic aberration)

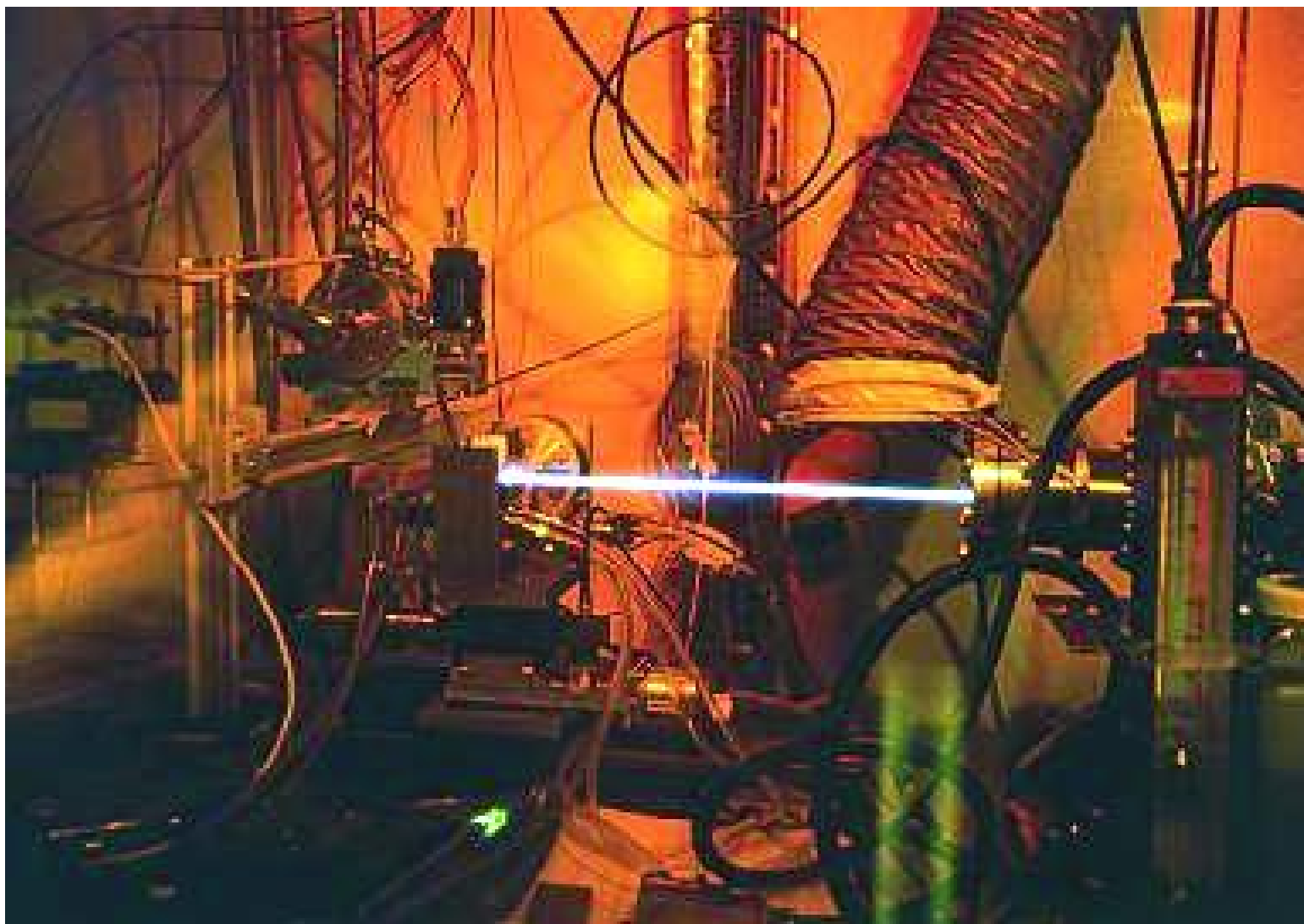


What is light sources from Accelerator?



- 광속으로 달리는 전자가 자기장 속을 지나면서 방향을 틀 때 접선방향으로 방출되는 아주 강력한 빛(**high energy photons**)을 말한다.
- 포항방사광 가속기는 태양보다 10억 배 이상 밝다.
- 방출되는 빛은 가시광선은 물론 자외선에서 X선에 이르는 모든 파장을 망라한다.

Synchrotron radiation



Beamline

- Leads to the experimental endstation utilizing particle beams from a particle accelerator, synchrotron light .
- Major parts of beam lines are **mirrors** and **spectroscopes**.



PLS Beamline Status

OCTOBER 2006

PLS Beamline Status



Construction	-----	4 beamlines
Commissioning	=====	1 beamlines
Operation	—————	26 beamlines

*Technical Building II : 펄스초-원적외선 (fs-FIR)

포항 방사광 가속기

- 우리나라 최대의 본격적인 가속기
- **제 3세대형** : 삽입장치를 최대한 사용
- 방사광 발생용 저장링 : **2.5 GeV**
 - 둘레 280 m, 세계 4위급
- 입사용 선형가속기 : 2.5 GeV
 - 길이 160 m, 세계 3위급
- 1988년부터 설계 시작, 1994년 완성
- 총 건설비 : 1500억원
 - 포철 900억, 정부 600억 지원
- 매년 약 180억원의 운영비는 정부 지원

Characterizing the structure - radial distribution function, also called pair distribution function

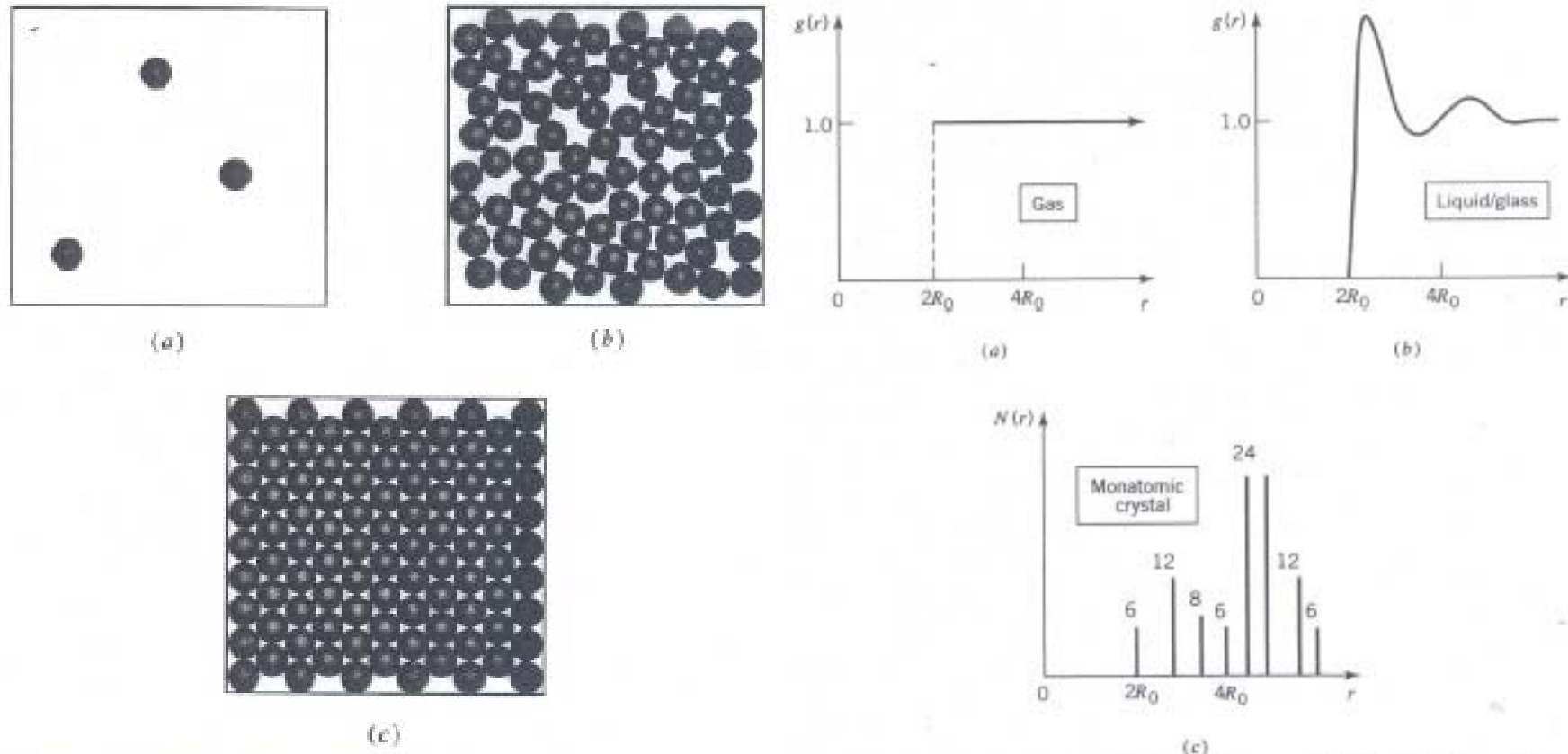
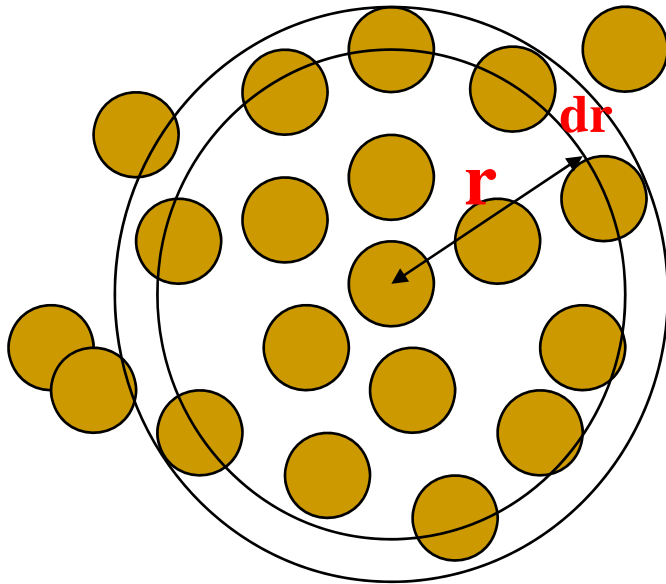


Figure 2.4 Hard-sphere model of (a) gas, (b) liquid/glass, and (c) crystalline solid.

Figure 2.5 Pair-distribution functions for (a) a gas and (b) liquid or glass. (c) The radial dependence of the number of neighbors $N(r)$ for a primitive cubic crystal with one atom per lattice site.

Gas, amorphous/liquid and crystal structures have very different radial distribution function

Radial distribution function - definition



$$g(r) = \frac{1}{\langle \rho \rangle} \frac{dn(r, r + dr)}{dv(r, r + dr)}$$

1. Carve a shell of size r and $r + dr$ around a center of an atom.

The volume of the shell is

$$dv = 4\pi r^2 dr$$

1. Count number of atoms with centers within the shell (dn)
2. Average over all atoms in the system
3. Divide by the average atomic density $\langle \rho \rangle$

RDF: count the neighbors

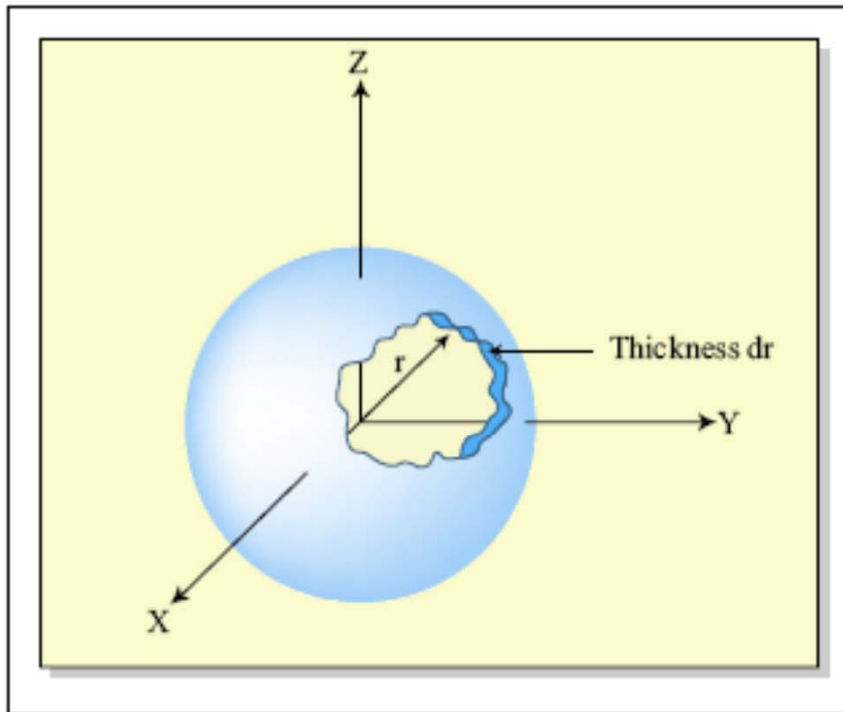
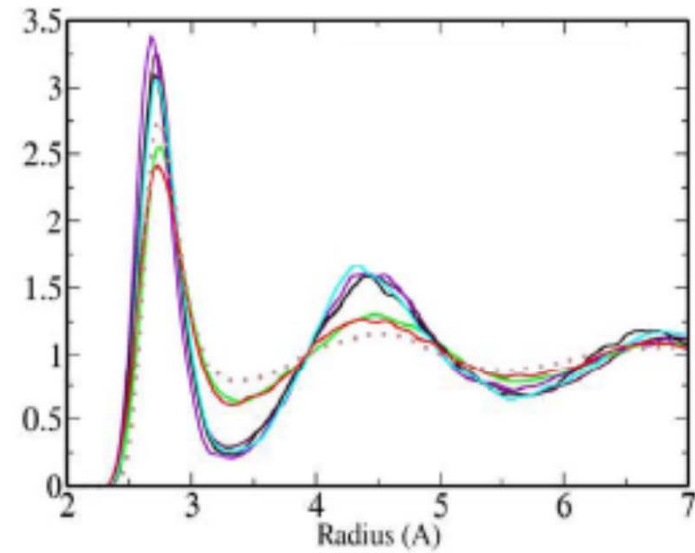


Figure by MIT OCW.



Properties of the radial distribution function

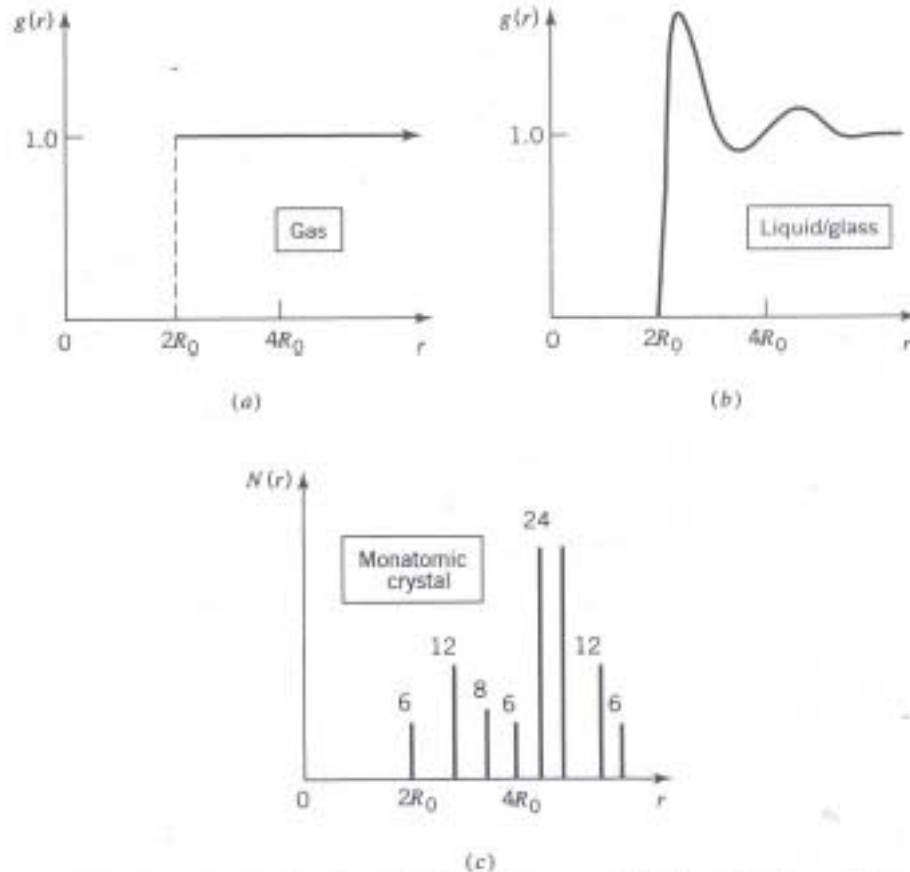


Figure 2.5 Pair-distribution functions for (a) a gas and (b) liquid or glass. (c) The radial dependence of the number of neighbors $N(r)$ for a primitive cubic crystal with one atom per lattice site.

For gases, liquids and amorphous solids $g(r)$ becomes **unity** for large enough r .

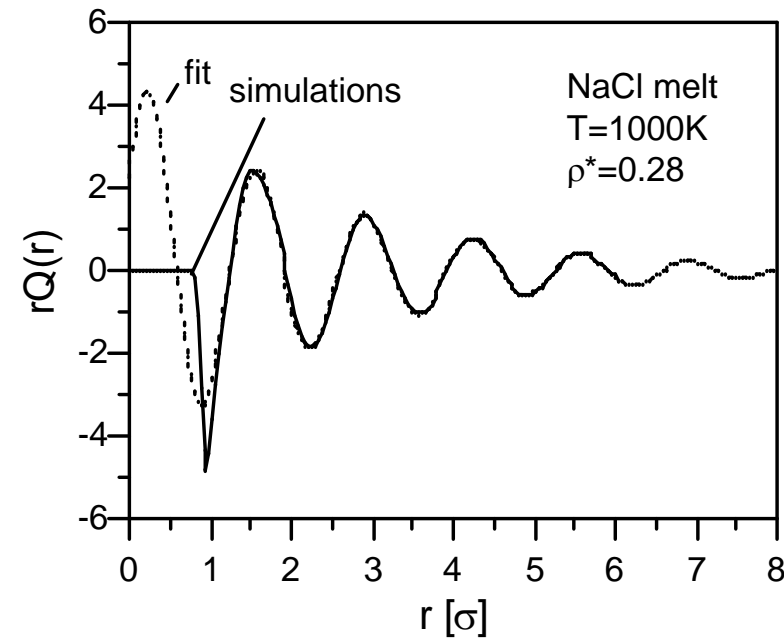
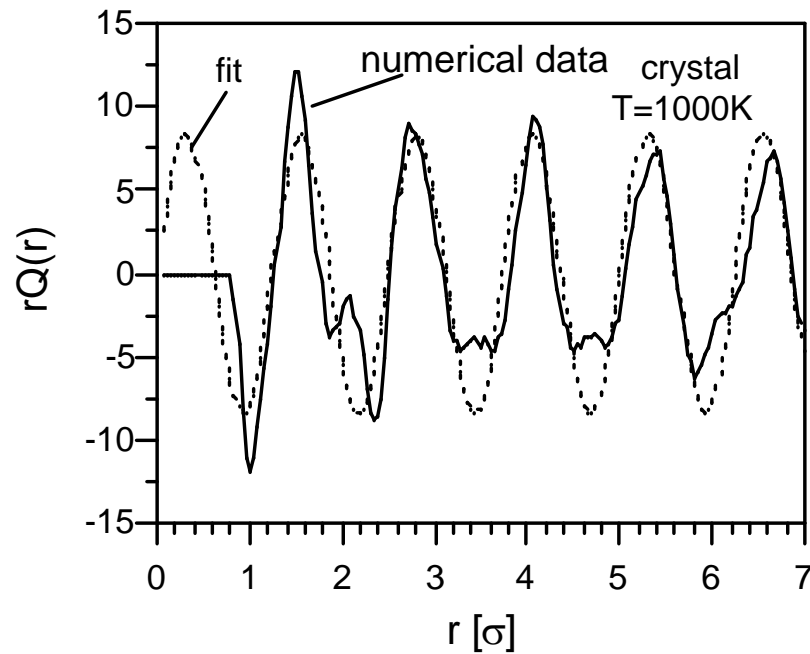
Features in $g(r)$ for liquids and amorphous solids are due to packing (exclude volume) and possibly bonding characteristics.

The distance over which $g(r)$ becomes unity is called the correlation distance which is a measure of the extent of so-called **short range order (SRO)**

The first peak corresponds to an average nearest neighbor distance.

Radial Distribution Function - Crystal and Liquid

$$Q(r) = g(r) - 1 \sim \frac{1}{r} \sin(r/d + \varphi) \exp(r/\lambda)$$



- Liquid/amorphous $g(r)$, for large r exhibit oscillatory exponential decay.
- Crystal $g(r)$ does not exhibit an exponential decay ($\lambda \rightarrow \infty$).

Radial distribution functions and the structure factor

- **The structure factor, $S(k)$** , which can be measured experimentally (e.g. by X-rays) is given by the **Fourier transform of the radial distribution function** and vice versa.

$$S(k) = 1 + \frac{4\pi\langle\rho\rangle}{k} \int_0^{\infty} r[g(r) - 1] \sin(kr) dr$$

Radial distribution functions can be obtained from experiment and compared with that from the structural model.

 More detailed structural characterization - Voronoi Polyhedra

Your Assignment V: study and summary for Voronoi Polyhedra and submit as a ppt file (under 5 pages)

5.2 Methodology

5.2.1 Transformation Temperatures

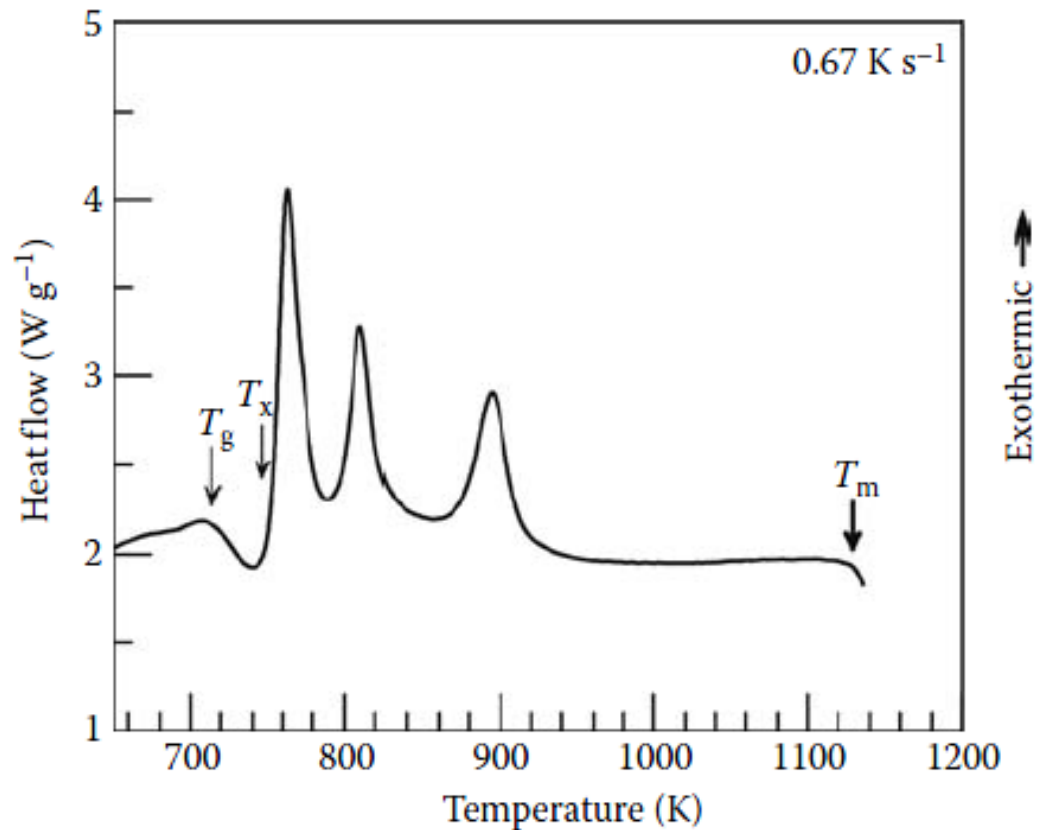
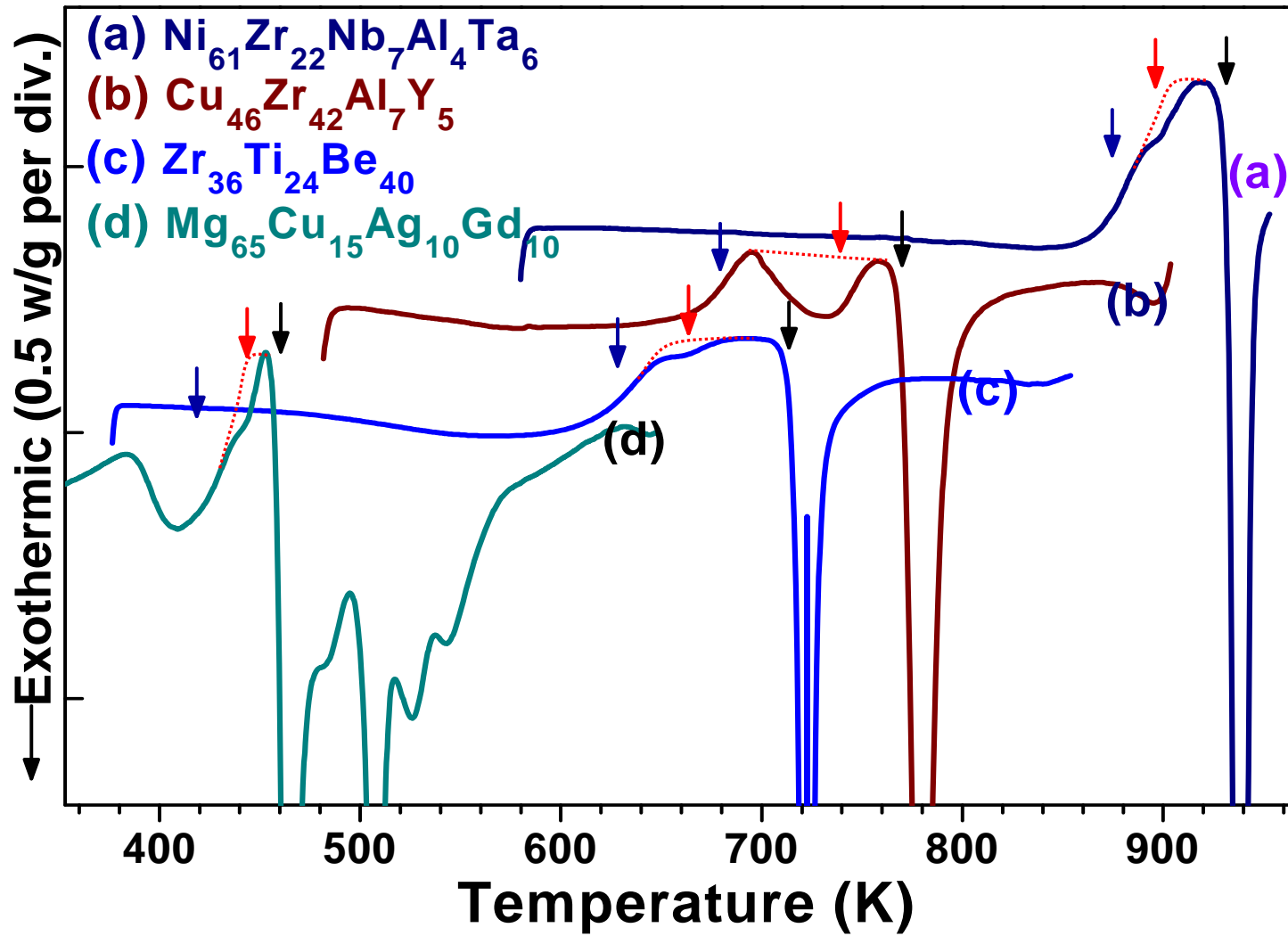


FIGURE 5.1

Schematic of a typical differential scanning calorimeter (DSC) curve obtained on heating a BMG alloy from room temperature to high temperatures at a constant heating rate of 40 K min⁻¹. Note that the curve displays three important temperatures—the glass transition temperature, T_g , the crystallization temperature, T_x , and the melting temperature, T_m . In some cases, there may be more than one crystallization temperature, depending upon the number of stages in which the glass or the supercooled liquid transforms into the crystalline phase(s).

Variation of T_g depending on alloy compositions → Broken Bonds



→ Almost all of the BMGs exhibit T_g . But, there are a few exceptions to this. For example, Nd-Fe-Al and Pr-Fe-Al glassy alloys did not exhibit any T_g , even though $D_{\max} > 10$ mm.

TABLE 5.1

Transformation Temperatures Determined for Some Typical BMG and Melt-Spun Glassy Alloys

Composition	Glass-Forming Technique		T_g (K)	T_x (K)	ΔT_x ($= T_x - T_g$) (K)	Heating Rate ($K s^{-1}$) ^a
Au ₅₅ Cu ₂₅ Si ₂₀	Cu-mold casting	low	348	383	35	0.33
Ca _{66.4} Al _{33.6}	Cu-mold casting		528	540	12	0.33
Ca ₆₀ Al ₃₀ Ag ₁₀	Cu-mold casting		483	531	48	0.33
Ca ₅₈ Al ₃₂ Mg ₁₀	Cu-mold casting		513	539	26	0.33
Ca ₆₅ Mg ₁₅ Zn ₂₀	Cone-shaped Cu-mold casting		374	412	38	0.67
Ce ₆₀ Al ₁₀ Ni ₁₀ Cu ₂₀	Suction casting		374	441	67	0.167
Co ₄₃ Fe ₂₀ Ta _{5.5} B _{31.5}	Cu-mold casting	high	910	982	72	0.67
Cu ₅₀ Zr ₅₀	Cu-mold casting		675	732	57	0.67
Cu ₅₀ Zr ₅₀	Melt spinning		686	744	58	0.67
Cu ₆₀ Zr ₃₀ Ti ₁₀	Cu-mold casting (2.5 mm dia rod)		714	758	44	0.67
Cu ₆₀ Zr ₃₀ Ti ₁₀	Melt spinning		711	754	43	0.67
Cu ₄₆ Zr ₄₂ Al ₇ Y ₅	Injection casting into Cu-mold (10 mm dia rod)		672	772	100	0.33
Fe ₆₄ Mo ₁₄ C ₁₅ B ₇	Injection casting into Cu-mold (2.5 mm dia rod)		793	843	50	0.33
Hf _{52.5} Cu _{17.9} Ni _{14.6} Al ₁₀ Ti ₅	Suction casting		767	820	53	0.167
La ₅₅ Al ₂₅ Ni ₁₀ Cu ₁₀	High-pressure die casting (9 mm dia rod)		460	527	67	0.67
La ₅₅ Al ₂₅ Ni ₁₀ Cu ₁₀	Melt spinning		460	550	90	0.67
Mg ₆₅ Cu _{7.5} Ni _{7.5} Zn ₅ Ag ₅ Y ₁₀	Melt spinning		430	459	29	0.67
Ni _{60.25} Nb _{39.75}	Injection casting into Cu-mold (1 mm dia rod)		891	923	32	0.33
Ni ₆₂ Nb ₃₃ Zr ₅	Injection molding (3 mm dia rod)		877	917	40	0.33
Pd ₇₉ Ag ₄₅ Si _{16.5}	Splat cooling		640	672	32	0.33
Pd ₇₈ Ag _{5.5} Si _{16.5}	Dropping a molten droplet onto metal substrate		642	683	41	0.33
Pd ₈₀ Au _{3.5} Si _{16.5}	Splat cooling		644	675	31	0.33
Pd ₇₈ Au ₄ Si ₁₈	Roller quenching		656	696	40	0.67

TABLE 5.1

Transformation Temperatures Determined for Some Typical BMG and Melt-Spun Glassy Alloys

Composition	Glass-Forming Technique	T_g (K)	T_x (K)	ΔT_x ($= T_x - T_g$) (K)	Heating Rate ($K s^{-1}$) ^a
Pd ₄₃ Cu ₂₇ Ni ₁₀ P ₂₀ (fluxed)	Water quenching	585	716	largest 131	0.67
Pd ₄₃ Cu ₂₇ Ni ₁₀ P ₂₀ (foam)	Water quenching	577	667	90	0.33
Pd ₄₀ Cu ₃₀ Ni ₁₀ P ₂₀ (unfluxed)	Melt spinning	572	663	91	0.33
Pd ₄₀ Cu ₃₀ Ni ₁₀ P ₂₀ (fluxed)	Melt spinning	572	670	98	0.33
Pd _{77.5} Cu ₆ Si _{16.5}	Dropping a molten droplet onto metal substrate	646	686	40	0.33
Pd ₄₀ Ni ₄₀ P ₂₀	Centrifugal spinning	583	650	67	0.33
Pd ₄₀ Ni ₄₀ P ₂₀ (fluxed)	Water quenching (7 mm dia rod)	576	678	102	0.33
Pd ₄₀ Ni ₄₀ P ₂₀ (unfluxed)	Melt spinning	580	643	63	0.33
Pd ₄₀ Ni ₄₀ P ₂₀ (fluxed)	Melt spinning	590	671	91	0.33
Pd ₈₁ Si ₁₉ (fluxed)	Air cooling	638	696	58	0.33
Pd ₈₁ Si ₁₉ (fluxed)	Melt spinning	633	675	42	0.33
Pd ₈₀ Si ₂₀	Splat cooling	655	667	12	0.33
Pr ₆₀ Cu ₂₀ Ni ₁₀ Al ₁₀	Suction casting	409	452	43	0.167
Pt _{57.5} Cu _{14.7} Ni _{5.3} P _{22.5} (fluxed)	Water quenching (16 mm dia rod)	508	606	98	0.33
Sm ₅₆ Al ₂₂ Ni ₂₂	Suction casting	544	582	38	0.33
Ti ₃₂ Hf ₁₈ Ni ₃₅ Cu ₁₅	Planar flow casting	722	766	44	0.167
Ti ₅₀ Ni ₂₄ Cu ₂₀ B ₁ Si ₂ Sn ₃	Cu-mold casting	726	800	74	0.67
Ti ₄₀ Zr ₂₅ Ni ₂ Cu ₁₃ Be ₂₀	Cu-mold casting	599	644	45	0.33
Y ₃₆ Sc ₂₀ Al ₂₄ Co ₂₀	—	645	760	115	0.67
Zr ₆₅ Al _{7.5} Ni ₁₀ Cu _{17.5}	Water quenching (16 mm dia rod)	625	750	125	0.67
Zr ₆₅ Al _{7.5} Ni ₁₀ Cu _{17.5}	Melt spinning	622	749	127	0.67
Zr _{41.2} Ti _{13.8} Cu _{12.5} Ni ₁₀ Be _{22.5}	Cu-mold casting	625	705	80	0.33

^a 0.167 K s⁻¹ = 10 K min⁻¹; 0.33 K s⁻¹ = 20 K min⁻¹; and 0.67 K s⁻¹ = 40 K min⁻¹.

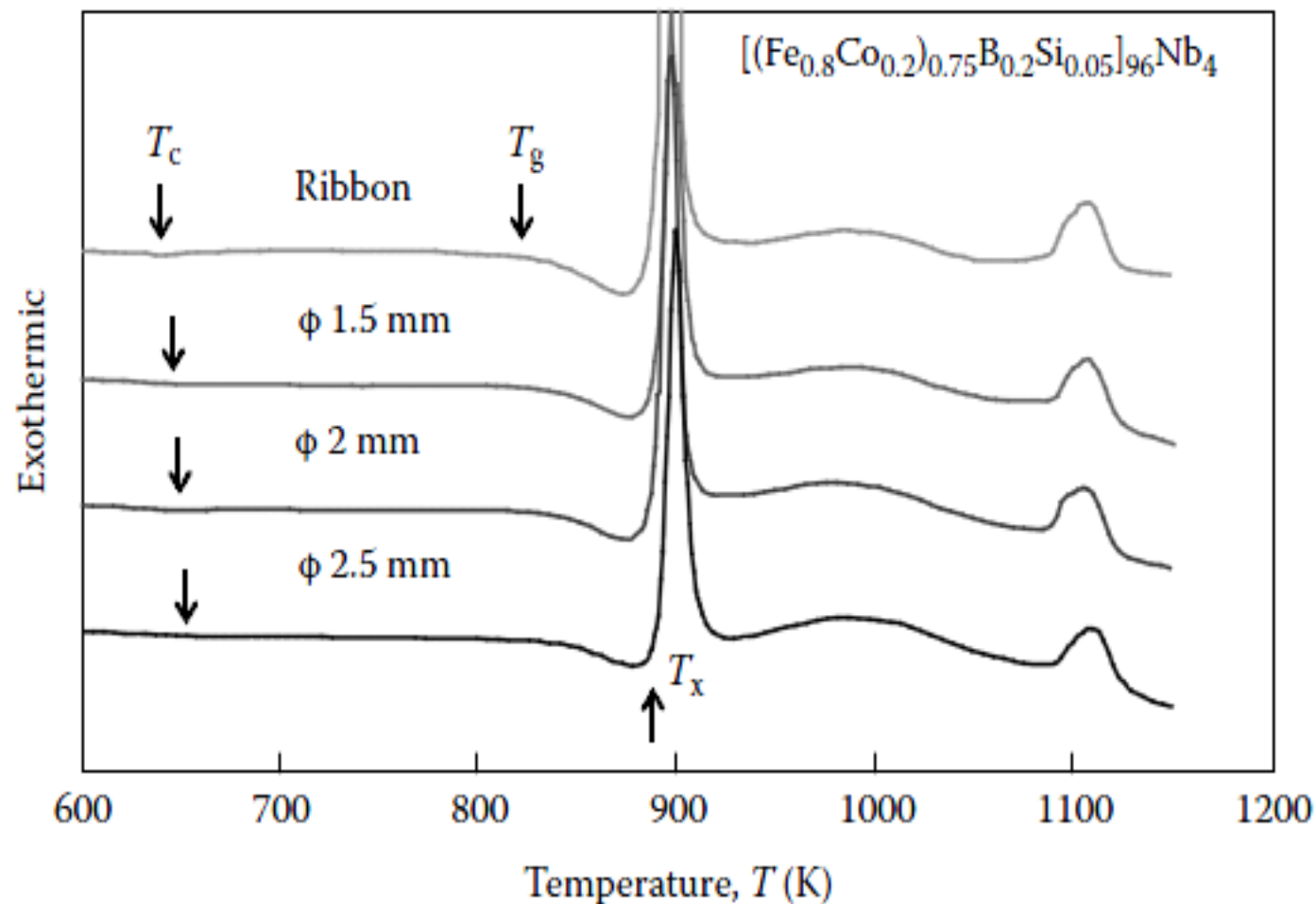
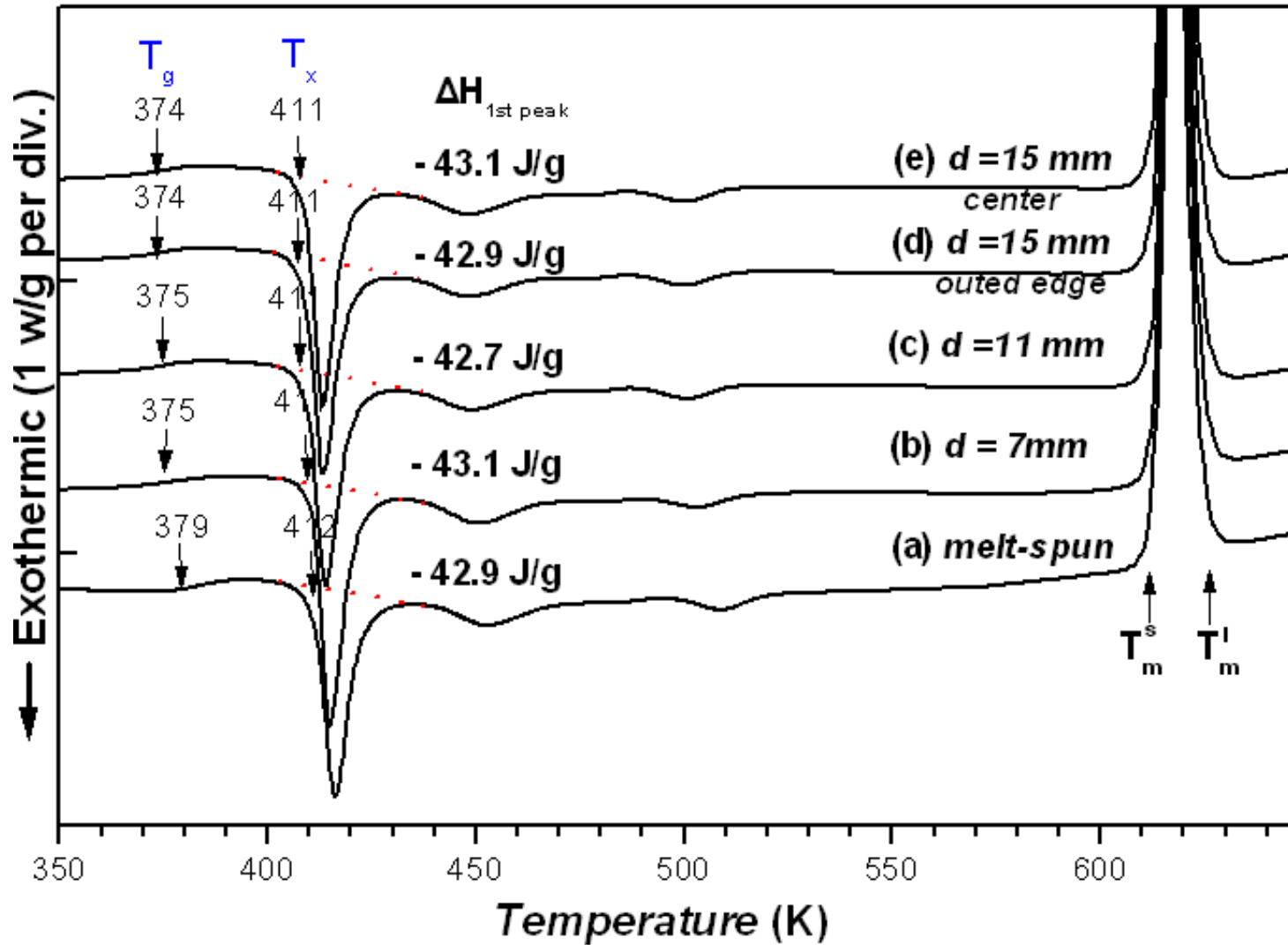


FIGURE 5.2

DSC curves of bulk glassy $[(\text{Fe}_{0.8}\text{Co}_{0.2})_{0.75}\text{B}_{0.2}\text{Si}_{0.05}]_{96}\text{Nb}_4$ alloy of different diameters (1.5, 2.0, and 2.5 mm) and melt-spun ribbon of the same composition. These curves clearly demonstrate that the transformation temperatures are identical for all the samples and that the transformation temperatures do not depend upon the diameter of the rod or the thickness of the ribbon.

(Reprinted from Inoue, A. et al., *Acta Mater.*, 52, 4093, 2004. With permission.)

*** Typically T_g is ~ 50-60% of the melting point.**



* J Mater Res, 19 (2004) 685.

The glass transition temperature T_g is a kinetic parameter and its value depends on the cooling rate at which the glass is formed (and also on the heating rate at which the glassy sample is reheated). It was also noted that T_g was lower when the glass had formed at lower cooling rates. Therefore, it would be possible to assume that the T_g for the melt-spun ribbon and BMG rod will be different. But, this is not true. The reason is that T_g , the temperature at which the glass is formed is estimated during the cooling of the molten alloy. On the other hand, T_g is usually measured experimentally during the heating of the glassy alloy that has already formed. Once the glass is heated from room temperature to higher temperatures, it is structurally relaxed and, therefore, it does not matter how the glass had initially formed. Accordingly, both types of glasses will have the same T_g and T_x temperatures, when measured at the same heating rate. That is, there is no difference between the T_g values of glasses prepared by RSP or slow solidification methods.

5.4 Differences in the Crystallization Behavior between Melt-Spun Ribbons and Bulk Metallic Glasses

- (a) The melt-spun metallic glass ribbons **solidified at higher cooling rates** are farther from equilibrium than the BMGs. → **a larger decrease in density and higher energy stored** in the melt-spun ribbons → One would expect that, **due to the larger departure from equilibrium, the kinetics of crystallization in melt-spun glassy ribbons would be faster than that in BMGs. But this is not necessarily true.**
- (b) Once the glass is heated to a temperature above T_g , the glass **becomes a supercooled liquid** (but still exists in the form of a solid). At this stage there is **no difference in the “structure”** between the BMG and the melt-spun metallic glass that was obtained directly by rapidly solidifying the metallic melt, **except that the extent of structural relaxation would be different in the two glasses.** → Therefore, once the BMG has been heated to **above T_g , the crystallization behavior of BMGs and melt-spun metallic glassy ribbons will be identical** (assuming that both the glasses have the same chemical composition).

5.2.2 Activation energy for crystallization

Two different methods: (a) Kissinger method, (b) Ozawa method

(a) Kissinger method $\ln\left(\frac{\beta}{T_p^2}\right) = \left(-\frac{Q}{RT_p}\right) + A$ where
 A is a constant
 R is the universal gas constant

Thus, by plotting $\ln(\beta/T_p^2)$ against $1/T_p$, one obtains a straight line whose slope is $-Q/R$, from which the activation energy for the transformation, Q can be calculated (Figure 5.3).

- Could get the required data during continuous heating in a DSC
- Possible to evaluate the individual activation energies for the nucleation and growth stages of the transformation
- May not be useful in all studies of decomposition

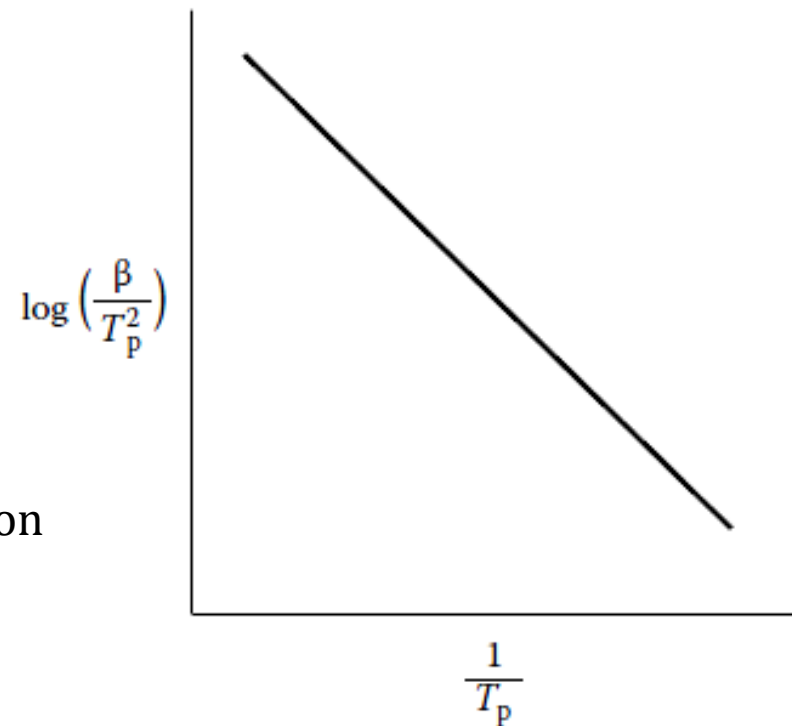


FIGURE 5.3

Kissinger plot in which $\ln(\beta/T_p^2)$ is plotted against $1/T_p$, when a straight line is obtained. The activation energy for crystallization can be calculated from the slope of this straight line.

* Overall Transformation Kinetics – TTT Diagram

By recording the isothermal DSC scans at different temperatures,
The fraction of Transformation as a function of Time and Temperature

$$\rightarrow f(t, T)$$

Plot f vs $\log t$.

- isothermal transformation

- $f \sim$ volume fraction of β at any time; $0 \sim 1$

Plot the fraction of transformation (1%, 99%) in T- $\log t$ coordinate.

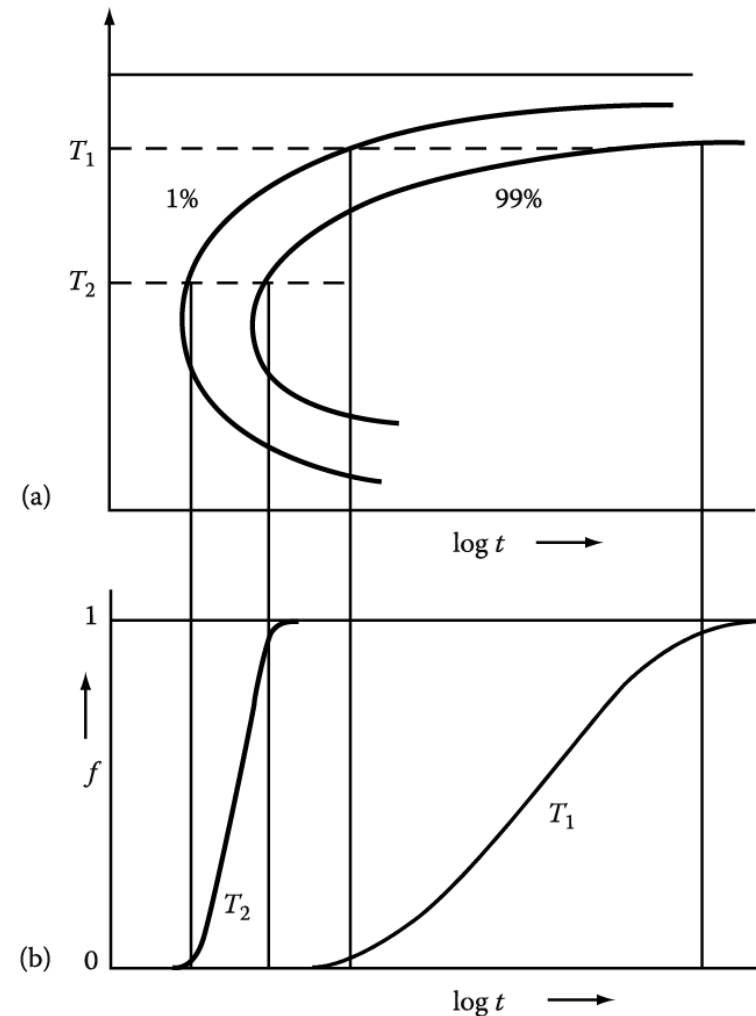
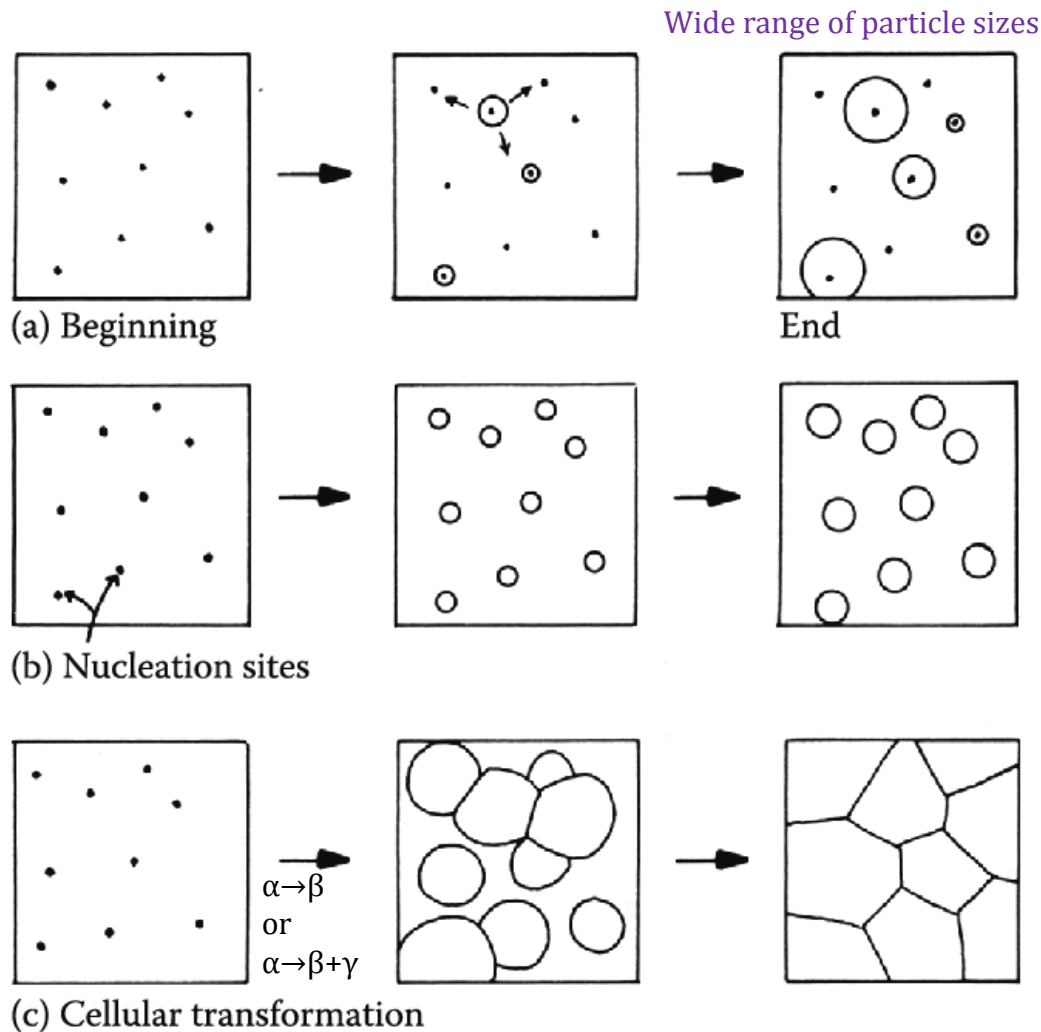


Fig. 5.23 The percentage transformation versus time for different transformation temperatures.

$f(t,T)$ 에 영향을 미치는 인자: 핵생성 속도, 성장 속도, 핵생성 자리의 밀도와 분포, 인접 지역에서의
 변태에 의한 확산영역의 중첩, 변태된 상 사이의 충돌 등
 몇가지 예,

Three Transformation Types



(a) continuous nucleation

Metastable α phase with many nucleation sites by quenching to T_t

→ f depends on the nucleation rate and the growth rate.

(b) all nuclei present at $t = 0$

→ f depends on the number of nucleation sites and the growth rate.

(c) All of the parent phase is consumed by the transformation product.

Transformation terminate by the impingement of adjacent cells growing with a constant velocity.

→ pearlite, cellular ppt, massive transformation, recrystallization



Fig. 5.24 (a) Nucleation at a constant rate during the whole transformation.
 (b) Site saturation – all nucleation occurs at the beginning of transformation.
 (c) A cellular transformation.

Transformation Kinetics

- Avrami proposed that for a three-dimensional nucleation and growth process kinetic law

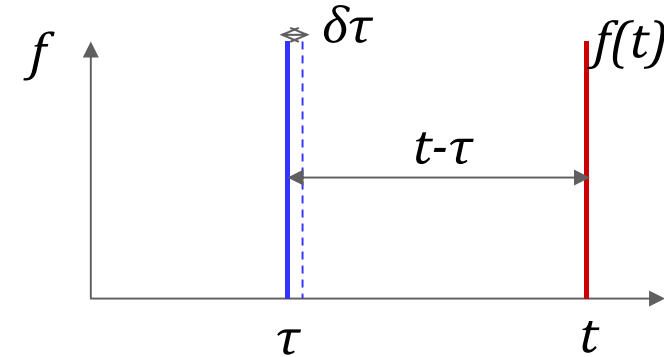
$$f = 1 - \exp(-kt^n) \quad \text{Johnson-Mehl-Avrami equation}$$

$$f: \text{volume fraction transformed} = \frac{\text{Volume of new phase}}{\text{Volume of specimen}}$$

- **Assumption :**
 - ✓ reaction produces by nucleation and growth
 - ✓ nucleation occurs randomly throughout specimen
 - ✓ reaction product grows rapidly until impingement

Constant Nucleation Rate Conditions

- Nucleation rate (I) is **constant**.
- Growth rate (v) is constant.
- No compositional change



$$df_e = \frac{\left(\begin{array}{l} \text{Vol. of one particle nucleated} \\ \text{during } d\tau \text{ measured at time } t \end{array} \right) \times \left(\begin{array}{l} \text{number of nuclei} \\ \text{formed during } d\tau \end{array} \right)}{\text{Volume of specimen}}$$

$$df_e = \frac{\frac{4}{3} \pi [v(t-\tau)]^3 \times (IV_0 d\tau)}{V_0}$$

$$f_e(t) = \int_0^t I \cdot \frac{4}{3} \pi [v(t-\tau)]^3 d\tau$$

$$= I \cdot \frac{4}{3} \pi v^3 \left[-\frac{1}{4} (t-\tau)^4 \right]_0^t = \frac{1}{3} \pi I v^3 t^4$$

$$V = \frac{4}{3} \pi r^3 = \frac{4}{3} \pi (vt)^3$$

$$V' = \frac{4}{3} \pi v^3 (t-\tau)^3$$

- do not consider impingement & repeated nucleation
- only true for $f \ll 1$

As time passes the β cells will eventually impinge on one another and the rate of transformation will decrease again.

Constant Nucleation Rate Conditions

- consider impingement + repeated nucleation effects

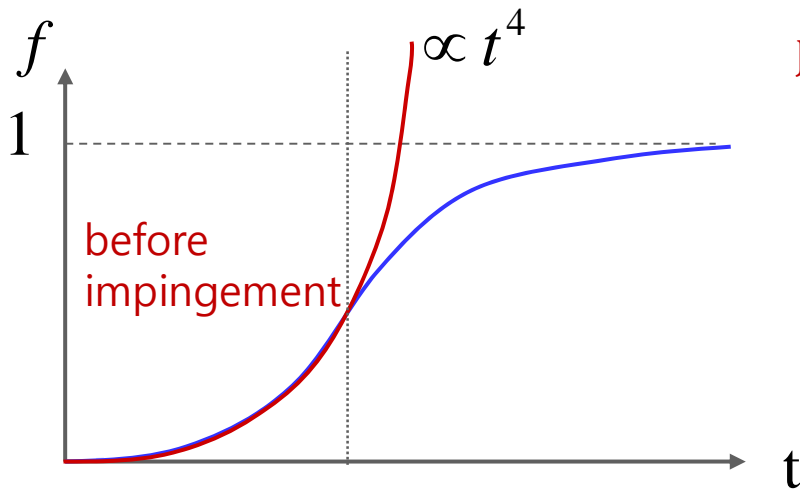
$$df = (1 - f)df_e \quad \longrightarrow \quad df_e = \frac{df}{1 - f}$$

$$f_e = -\ln(1 - f)$$

$$f(t) = 1 - \exp(-f_e(t)) = 1 - \exp\left(-\frac{\pi}{3} I v^3 t^4\right)$$

* Short time:
 $1 - \exp(z) \sim Z \quad (z \ll 1)$

* Long time:
 $t \rightarrow \infty, f \rightarrow 1$



Johnson-Mehl-Avrami Equation

$$f = 1 - \exp(-kt^n)$$

k : 온도에 민감함 $f(I, v) \quad -\frac{\pi}{3} I v^3$
 n : 1 ~ 4 (depend on nucleation mechanism)

Growth controlled. Nucleation-controlled.

상변태가 일어나는 동안 핵생성 기구에 변화가 없다면 n 은 온도에 무관.

$$\ln[-\ln\{1 - f(t)\}] = \ln k + n \ln(t) \quad (5.3)$$

Thus, by plotting $\ln[-\ln\{1 - x(t)\}]$ against $\ln(t)$, one obtains a straight line with the slope n .

- Chen & Spaepen (Harvard,1988)

a) *glass* → *nucleation & growth*
(perfect random)

→ Isothermal annealing
: rapid heating + maintain the temp.



- *Glass* :

J-M-A Eq. $x = 1 - \exp(-bt^n)$ (*n*: 2~4, nucleation mechanism)

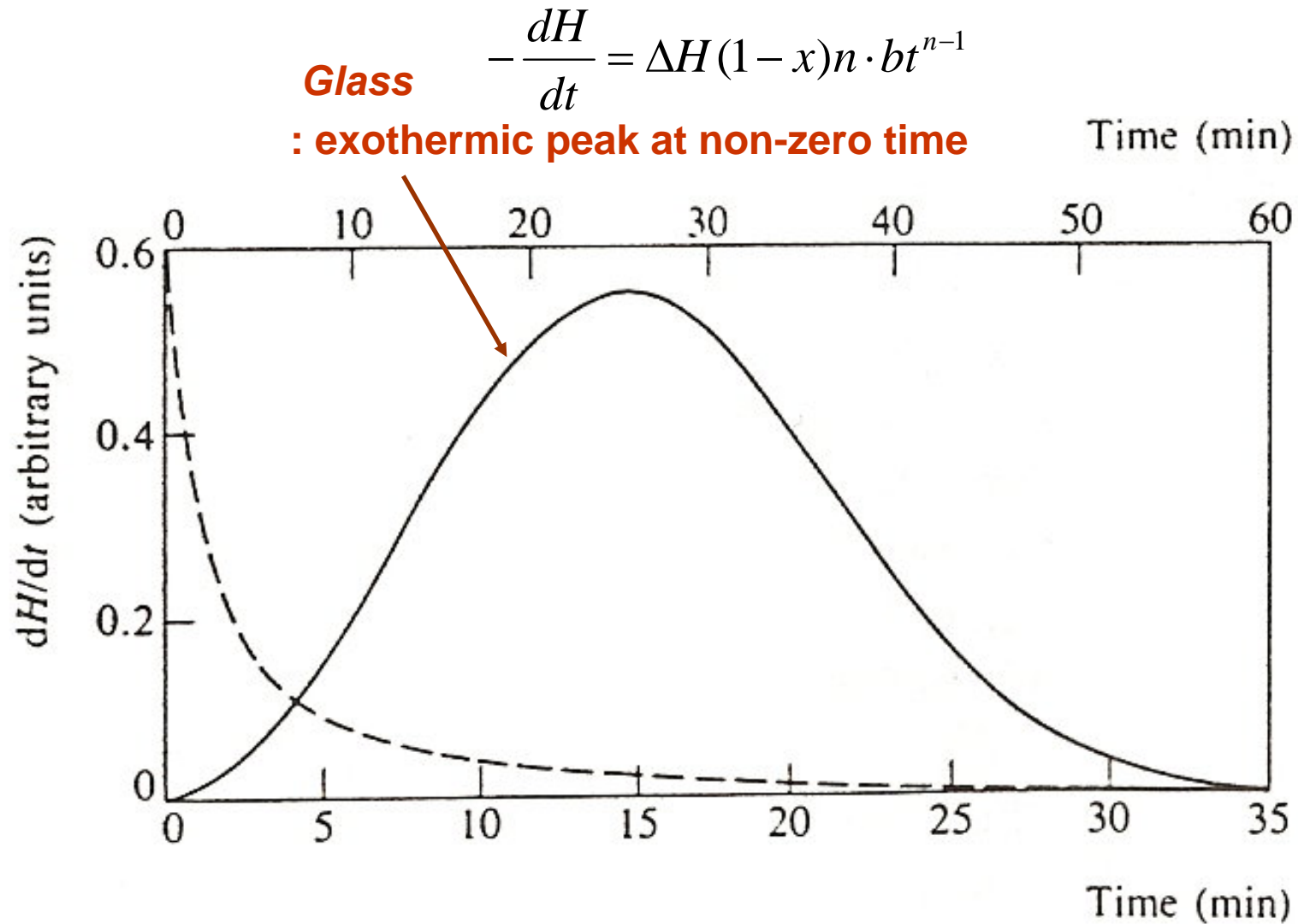
crystallized volume fraction after time t

→ *Corresponding heat release*

$$-\frac{dH}{dt} = \Delta H (1 - x)n \cdot bt^{n-1}$$

(ΔH : total transformation enthalpy)

Fig. 1.4 Isothermal enthalpy release rates for crystallite nucleation and growth (solid line) and crystallite grain-coarsening mechanisms (dashed line)



- **c) Nanocrystalline** → **grain growth**

$$\rightarrow \frac{dr}{dt} = M \cdot \frac{\gamma}{r^m}$$

(M: atomic mobility, γ : interfacial surface tension)

→ corresponding heat release

$$-\frac{dH}{dt} = H(0) \cdot r(0) \cdot M\gamma / r^{m+2}$$

(H(0): zero time enthalpy of a grain size of r (0))

→ Monotonically decreasing curve

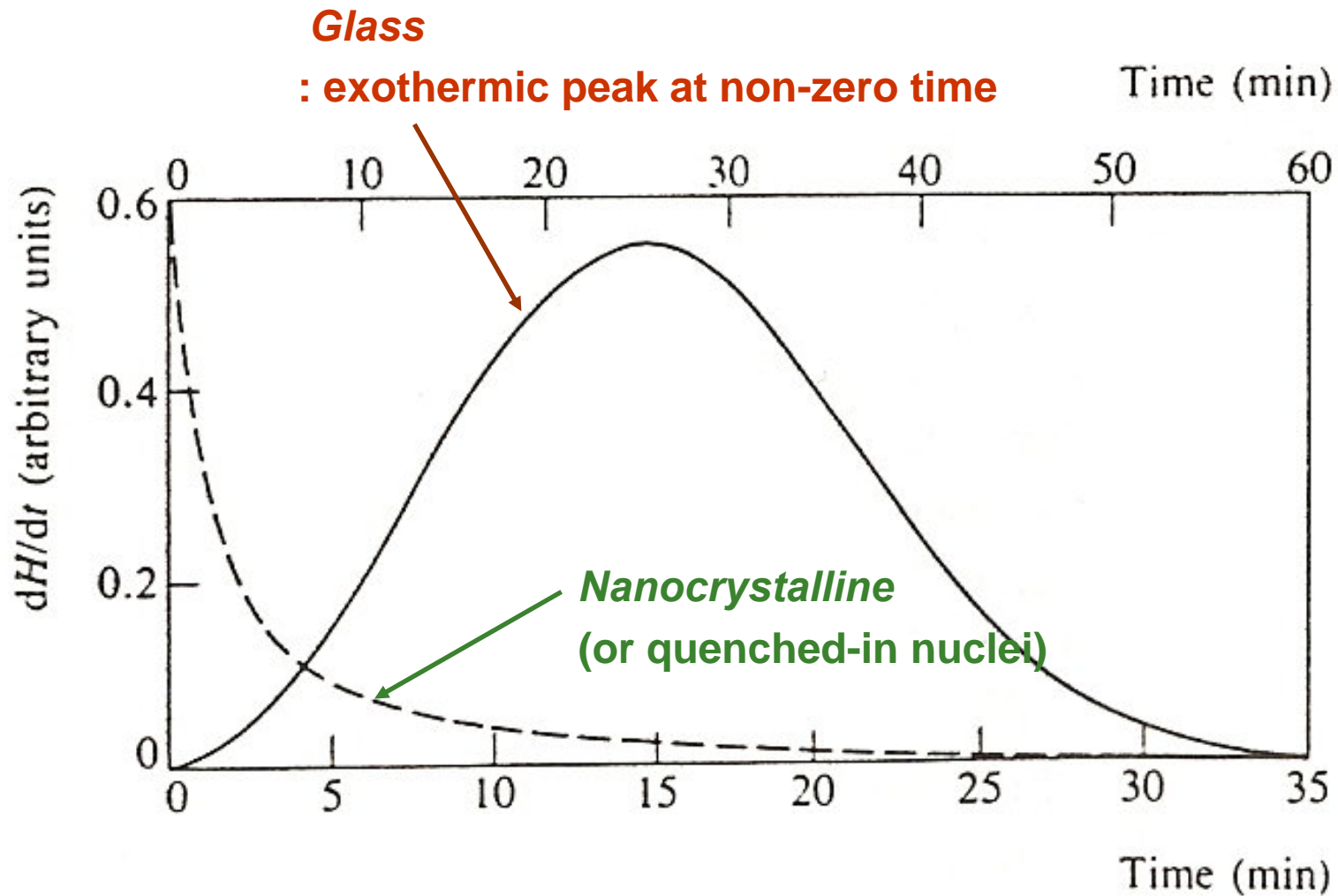


Fig. 1.4 Isothermal enthalpy release rates for crystallite nucleation and growth (solid line) and crystallite grain-coarsening mechanisms (dashed line)

Effect of quenched-in quasicrystal nuclei

● Isotherm in DSC

Isothermal annealing

